UNITED NATIONS UNIVERSITY
GEOTHERMAL TRAINING PROGRAMME
Orkustofnun, Grensasvegur 9,
IS-108 Reykjavik, Iceland

Reports 2012
Number 23

BOREHOLE GEOLOGY AND ALTERATION MINERALOGY OF WELL OW-914A, DOMES AREA, OLKARIA GEOTHERMAL FIELD, CENTRAL KENYA RIFT

Xavier Shioya Musonye
Kenya Electricity Generating Company, Ltd. – KenGen
P.O. Box 785 – 20117
Naivasha
KENYA
xmusonye@kengen.co.ke

ABSTRACT

Well OW-914A is a deviated production well drilled on the eastern margins of the Domes field in the Greater Olkaria geothermal area. This well is 2996 m deep with an inclination of 17.85° and azimuth N77.14°E. The well was drilled in order to confirm the resource east of the Domes area and to gather steam for the construction of the 140 MWe Olkaria IV power plant. The drilling was completed within 48 days, beginning 25th June 2010 and ending 11th August 2010. This report presents an analysis of the cuttings collected at 2 m interval from the surface to 2996 m depth in the well. According to binocular and petrographic analyses, it was observed that OW-914A cuts through lithological units mainly composed of pyroclastics, tuff, rhyolite, basalt and trachyte. Trachyte forms the bulk of the stratigraphy, predominantly below 900 m. One fine-grained basaltic dyke and seven fine-grained rhyolitic intrusions were observed. Alteration in the Domes area is mainly controlled by permeability, temperature and the primary rock type. Abundance of alteration minerals is highly related to the permeability and porosity of the formations. Higher temperature alteration minerals appear systematically with increasing depth in OW-914A. Five alteration zones were identified: - an un-altered zone (0-90 m), a zeolite-illite zone (90-480 m), a chlorite-illite zone (480-732 m), an epidote-chlorite-illite zone (732-1218 m) and an actinolite-epidote-chlorite-illite zone (1218-2996 m). Comparison of the hydrothermal mineral evolution sequences and fluid inclusion analysis show that the system has been in a state of equilibrium with only small temperature changes. However, there may have been a short lived boiling condition in the well at around 836 m depth, indicated by the fluid inclusion analysis. Thirteen feed zones were identified in this well, with the first one being identified at 90 m and the last one at 2940 m. The location of the feed zones correlates with fractures, fractured rhyolite rock, vesicular tuff, intrusions and lithological contacts. The main reservoir rock in the Domes area is trachyte. The trachyte has tuff, rhyolite and basalt intercalations. It is highly fractured but less porous, as indicated by the relative abundance of vein fillings but fewer vesicles in the drill cuttings.

1. INTRODUCTION

1.1 General information

The East African Rift System extends over 3000 km from the Red Sea at the Afar triple junction in the north and to Beira in Mozambique to the south. The Kenya Rift Valley is part of the eastern branch of the East African Rift System, which runs from Lake Turkana in Northern Kenya to Lake Natron in Northern Tanzania**.**

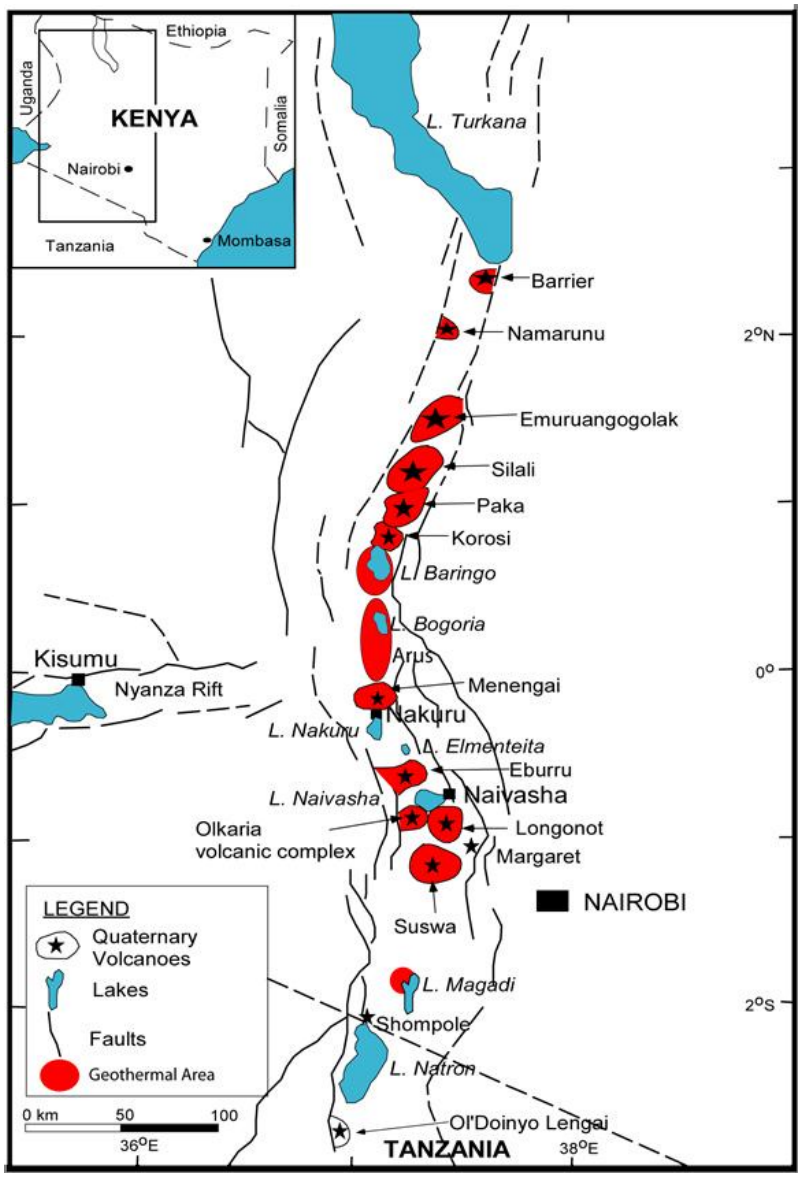

FIGURE 1: A map showing the location of Olkaria Volcanic Complex within the Kenyan Rift

The Greater Olkaria geothermal area, which lies within the Greater Olkaria volcanic complex, is located in the south central Kenyan Rift Valley, south of Lake Naivasha (Figure 1). OW-914A is situated in the Domes field of the Greater Olkaria geothermal area (Figure 2).

The Greater Olkaria geothermal area is sub-divided into seven smaller fields for the purposes of geothermal management (Figure 2). These are the Olkaria East, Olkaria North East, Olkaria Central, Olkaria Northwest, Olkaria Southwest, Olkaria Southeast and the Olkaria Domes fields. Most of these fields have been developed to a large extent, with several wells drilled that supply steam to the existing power plants. The 45 MWe are generated from the Olkaria East (Olkaria I) field, which was commissioned in 1981. It consists of 3 units, each producing 15 MWe. Olkaria Northeast (Olkaria II) generates 105 MWe and comprises three units producing 35 MWe each. Olkaria Northwest (Olkaria III) field generates 48 MWe and has been developed by an independent power producer (IPP). The construction of the fourth and fifth units of Olkaria I is currently underway. These units will have a total capacity of 140 MWe, with each unit generating 70 MWe. The Domes area has been extensively explored since 1998. Currently, a two-unit power plant is being constructed, also known as Olkaria IV, with a total capacity of 140 MWe. There is also the wellhead unit, commissioned in 2012, in the Olkaria East field, which generates 5 MWe. Olkaria central has been developed by a flower farm and generates 2 MWe.

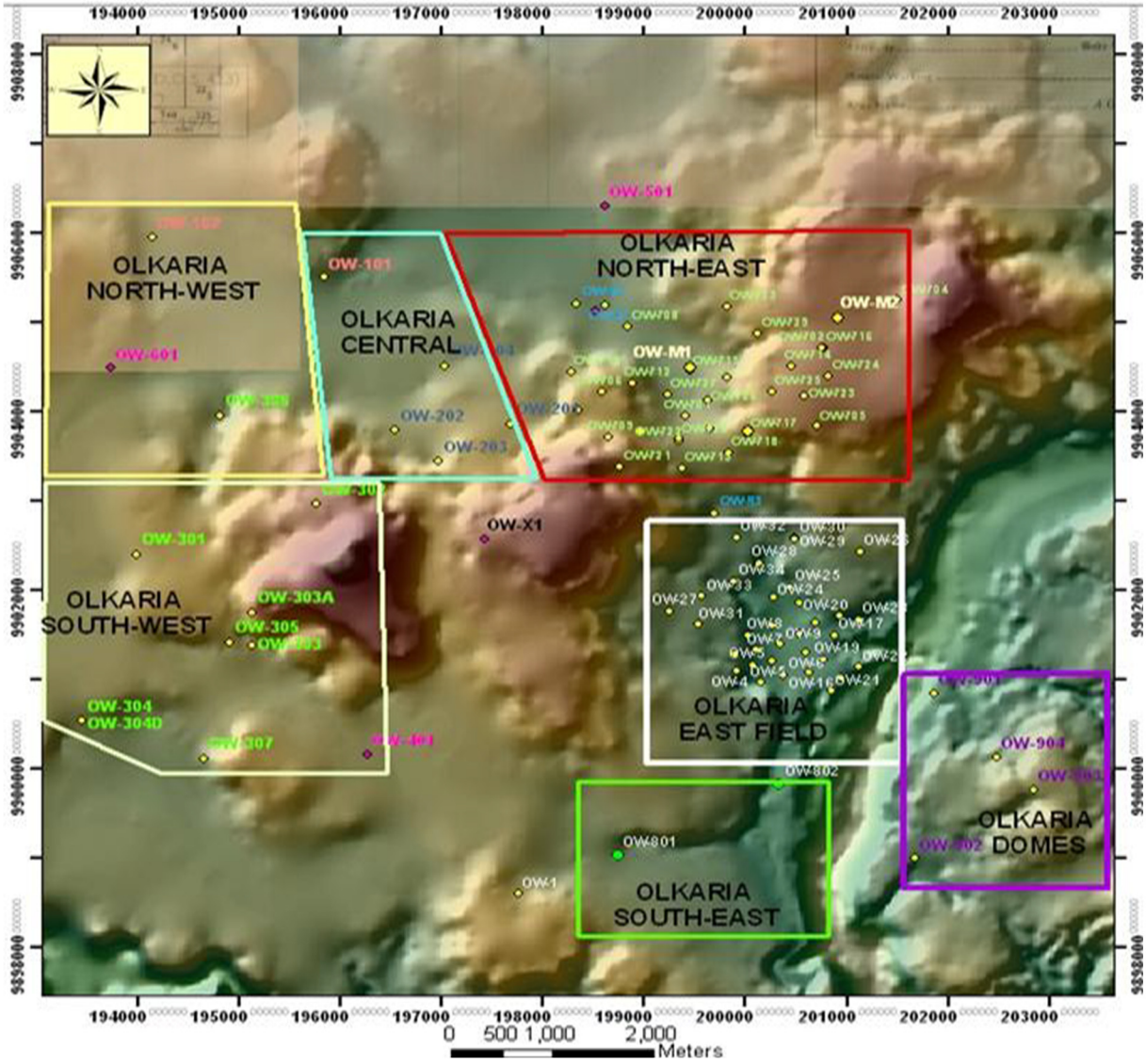

FIGURE 2: The seven divisions (fields) of the Greater Olkaria geothermal area (modified from KenGen, 2000)

1.2 Objectives of the study

The objectives of this study are: to delineate the lithological formations of well OW-914A, and to identify the alteration minerals and how they relate to the formation temperatures and feed zones of the well. These findings are used to delineate the distribution of aquifers with respect to the geological setting, while alteration mineral assemblages provide a guideline to set production casing depth for subsequent wells to be drilled in this area.

This study was presented as a requirement for the fulfilment of the six months postgraduate training course by the United Nations Geothermal Training Programme (UNU-GTP) attended in Iceland between May and October 2012.

2. GEOLOGY

2.1 Regional geology

The formation of the East African Rift system was initiated by the rift fault structure, which exploited the weak collision zone at the contact between the Archean Tanzanian craton and the Proterozoic orogenic belt (Smith and Mosely, 1993). The Kenya Rift Valley forms a segment of the eastern branch of the East African rift system. It straddles the margins of the Tanzanian craton and the Mozambique mobile belt, formed during the Pan-African orogenic event in the late Proterozoic (Smith and Mosely, 1993). The evolution of the Kenyan rift dates back to early Miocene (30 Ma). It began at the Turkana Rift in Northern Kenya where the earliest volcanic rocks in the Kenya rift have been found (MacDonald et al., 2001). This rift lies at the northern terminus of the East African rift system. The rifting was initiated by a north to east elongated zone of crustal warping, commonly termed the "Kenya Dome" (Baker et al., 1972; Bechtel et al., 1987). This was deduced from the study of the shape and height of the eroded surface in Kenya and western Uganda and long-wavelength gravity data. From these studies, the attitude of the basement-cover contact and the radial deposition of the early Miocene flood lava indicate that the formation of the dome largely preceded volcanism and rifting. Since volcanism preceded the major rift faulting events, Baker and Wohlenberg (1971) proposed a model of the rifting process where the driving force was provided by the convecting asthenospheric mantle. Geochemical analyses of the rocks have also pointed to the convecting asthenospheric mantle as the driving force of the rifting process (Marshall et al., 2009).

The magmatism began at the Turkana rift in the north, migrating southwards through central and southern Kenya, finally reaching Northern Tanzania 5-8 million years ago. The magmatic process also developed and propagated north of Baringo, as indicated by MacDonald et al. (2001). Williams (1972) and Baker (1987) estimated the total volume of eruptive rocks associated with rifting within the Kenyan rift valley to be more than 220,000 km^3.

The Pliocene eruptions that followed the Miocene volcanics and the subsequent faulting are divided into four principal phases (Baker et al., 1988). These phases were coupled with faulting episodes, during which time most of the structural features evolved. The first phase was the wide-spread Mau-Kinangop tuff ash flows, (3.7-3.4 Ma). Major faulting occurred following the ignimbrite eruptions, which converted an earlier half graben to a graben. The second phase was the eruption of the Limuru flood trachyte (2.0-1.8Ma), which was initiated by the progressive inward migration of the fault zones. This migration resulted in the formation of step-faulted platforms (Mau escarpments) and the fissure eruptions of the Limuru trachyte flood lavas. Basalts and basaltic trachyandesites form the third and fourth phases, respectively (1.65-0.9Ma). These last two phases were triggered by faulting that followed the Limuru flood trachytes. This faulting was triggered by a convecting mantle, opening up fractures, which served as conduits for Quaternary volcanic activity of mafic to felsic composition (Baker et al., 1988).

The most intense volcanic activity occurred within the central sector of the rift. The volcanic succession in this area is thought to be about 5 km thick. This is inferred from seismic data analysis (Henry et al., 1990; Simiyu et al., 1995; 1997) and stratigraphic correlation (Baker et al., 1972).

2.2 Geology of the Greater Olkaria volcanic complex

The regional setting and stratigraphy of the Greater Olkaria volcanic complex has been described by Clarke et al. (1990). The greater Olkaria volcanic complex is characterised by small numerous volcanic sites of Quaternary age. These sites are estimated at a total number of 80. They occur as steep-sided domes formed of lavas and/or pyroclastic rocks, or as thick lava flows of restricted lateral extent. The Olkaria volcanic complex has been observed to be the only area within the Kenyan Rift with the occurrence of comenditic lavas on the surface (MacDonald et al., 2008; Lagat, 2004).

The Greater Olkaria volcanic complex is adjacent to other Quaternary volcanic centres which are approximately 50 km away from it. These include Eburru to the north and Longonot and Suswa to the east and south, respectively (Figure 3). Even though these neighbouring volcanoes have calderas of varying sizes, the Olkaria complex does not have an explicit caldera. However, the existence of a buried caldera within the Olkaria volcanic complex has been postulated by the presence of a ring of volcanic domes in the east, south and southwest of this complex (Mungania, 1992; Naylor, 1972; Clarke et al., 1990). Geophysical studies have been conducted in this area but not all have been consistent with this explanation. Seismic wave attenuation indicates anomalies coinciding with the proposed buried caldera rim (Simiyu et al., 1998). Other studies have failed to identify this margin: resistivity studies have recorded no anomalies at the proposed collapsed caldera rim (Onacha, 1993) and subsurface geology indicates, for example, the absence of ignimbrites which could have been associated with the caldera collapse (Omenda, 1998).

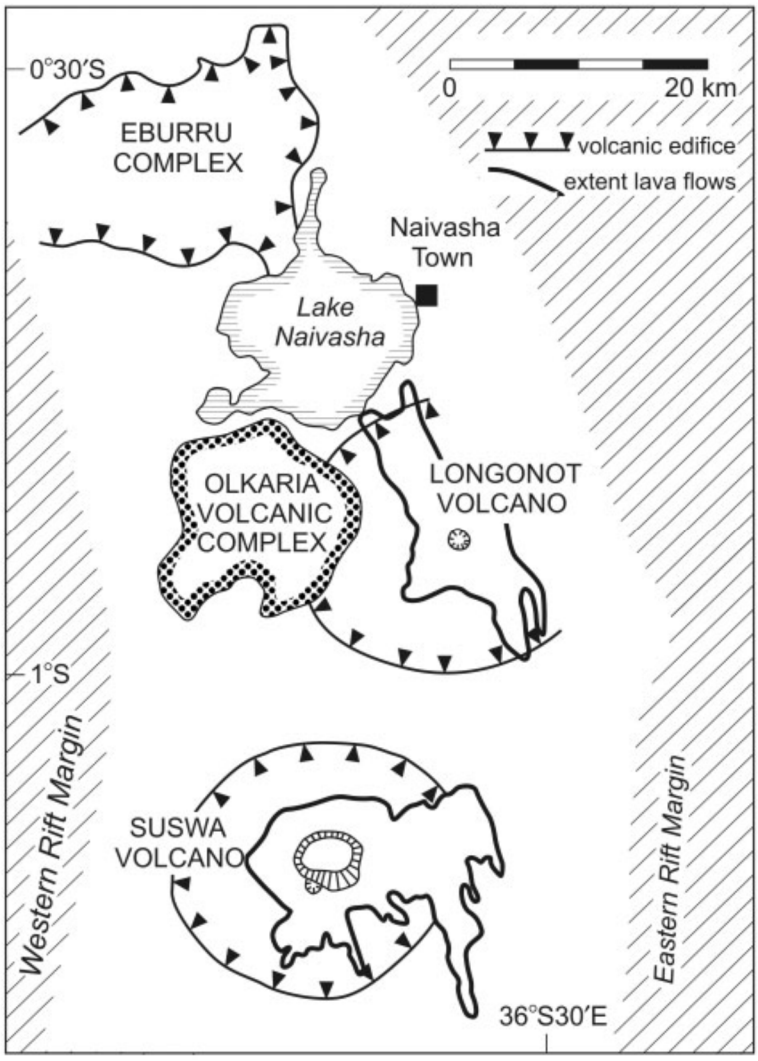

FIGURE 3: A map showing the location of Olkaria volcanic complex relative to adjacent volcanic complexes (from MacDonald et al., 2008)

The surface geology of the Olkaria volcanic complex is dominated by comenditic lava flows and pyroclastic deposits, while the subsurface geology is mainly characterised by basalts, trachytes, rhyolites and tuffs. Figure 4 shows the stratigraphic column, the age and age span of the Greater Olkaria volcanic complex. According to litho-stratigraphic studies obtained from drilled geothermal wells, the stratigraphy can be divided into six main groups (Omenda, 2000) which are connected with the six stages associated with the evolution of the East African Rift and the Olkaria volcanic complex. The six groups include: Proterozoic "basement" formations, Pre-Mau volcanics, Mau tuffs, Plateau trachytes, Olkaria basalt and Upper Olkaria volcanics.

The basement rocks, which are not exposed in this area except on the flanks of the south rift margins, mainly consist of amphibolite grade gneisses and schists, and associated marble and quartzite of the Mozambican Group (Shackleton, 1986). The estimated thickness of this group from the seismic studies carried out within the Central Kenyan rift is 5-6 km (Simiyu et al., 1995; Simiyu and Keller, 1997).

The Pre-Mau volcanics are not exposed in this area but only on the flanks of the southern rift. They are mainly composed of basalts, trachytes and ignimbrites. The Mau tuffs, which are consolidated and ignimbritic in texture, form the reservoir rocks of the Olkaria West field (Lagat, 2004). They are the oldest exposed rocks in the Olkaria area.

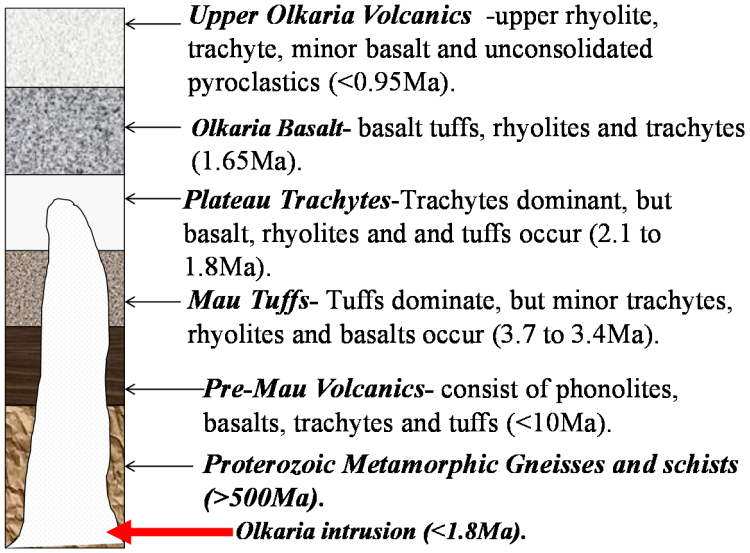

FIGURE 4: Stratigraphic column and age span of the Greater Olkaria volcanic complex (modified from Omenda, 2000)

The Plateau trachytes are composed of trachytic lavas with basalt, tuff and rhyolite intercalations. They comprise the geothermal reservoir rocks for the Olkaria East field where they dominate, occurring from between 1000 and 2600 m depth (Ogoso-Odongo, 1986; Omenda, 1994). Olkaria basalt consists of basalt flows, minor pyroclastic deposits and trachytes. It is believed to form the cap-rock for the Olkaria geothermal system (Haukwa, 1984; Ambusso and Ouma, 1991), and varies in thickness from 100 to 500 m, underlying the Upper Olkaria volcanics.

The Upper Olkaria volcanics are mainly composed of comenditic lavas and pyroclastic deposits. They occur from the surface down to about 500 m depth (Lagat, 2004). The youngest lava of the upper formation is the Ololbotut comendite lava, which was dated to 180±50 years BP (Clarke et al., 1990). Pyroclastic deposits from Suswa and Longonot volcanoes also form part of this Upper Olkaria formation. Figure 5 shows the conceptual model, the faults, fractures, up-flow zones and the feeder zones of the Greater Olkaria geothermal area.

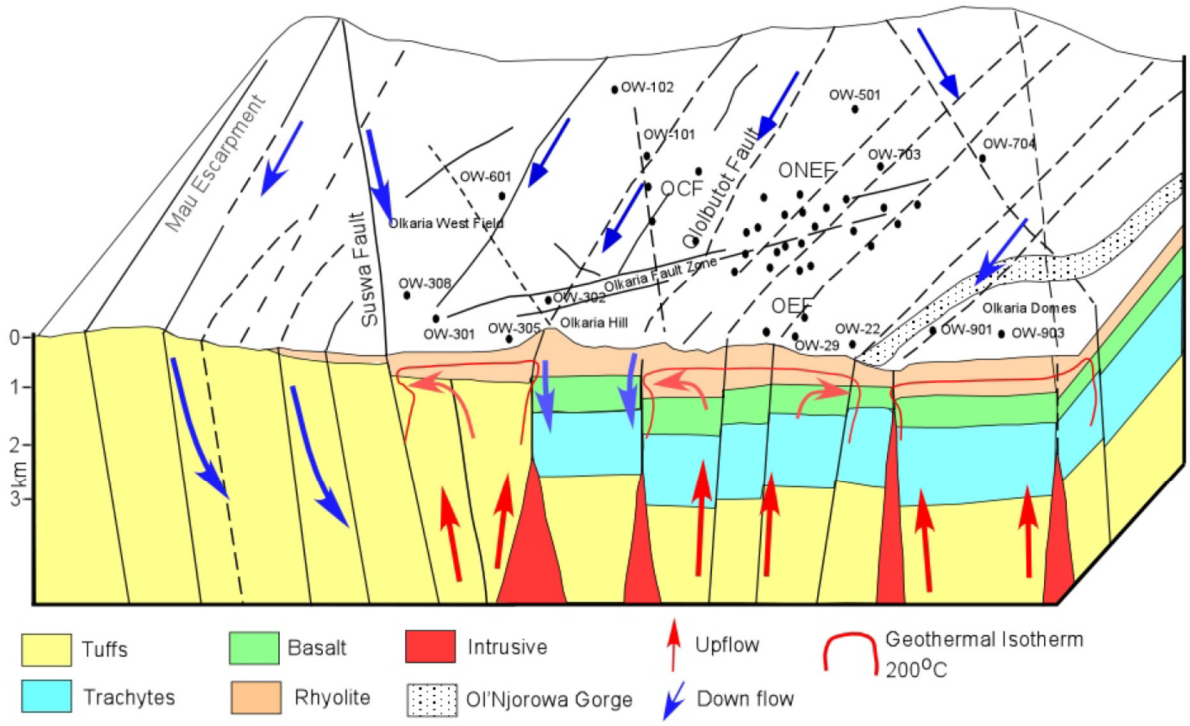

FIGURE 5: Conceptualized geothermal model of the Greater Olkaria geothermal area showing the general geology, structures and locations of the field with respect to recharge, up-flow and outflow zones (Mariita, 2009)

2.3 Tectonic structures of the Greater Olkaria volcanic complex

The Olkaria volcanic complex is located on the floor of the central southern segment of the Kenyan Rift Valley. The Olkaria geothermal field is located where a bend occurs in the Rift Valley from a NW-SE orientation to the north of Olkaria, to a N-S orientation of the Rift to the south of Olkaria geothermal field. The main tectonic structures in the Olkaria volcanic complex include fractures, faults, the Ol'Njorowa gorge and the ring structure. The main faults are: - the ENE-WSW Olkaria fault and the N-S Ololbutot fault, NNE-SSW, NW-SE and WNW-ESE trending faults (Figure 6). The faults are quite common in the East, Northwest and West Olkaria fields but are conspicuously absent in the Domes area. Their absence in the Domes area is attributed to a thick cover of pyroclastic material. However, through drilling, buried faults have been encountered in the Domes area. This has been indicated by cave-ins, circulation losses and, at other times, collapse of the wells during drilling, as seen in the recently drilled well OW-915B (KenGen, 2012).

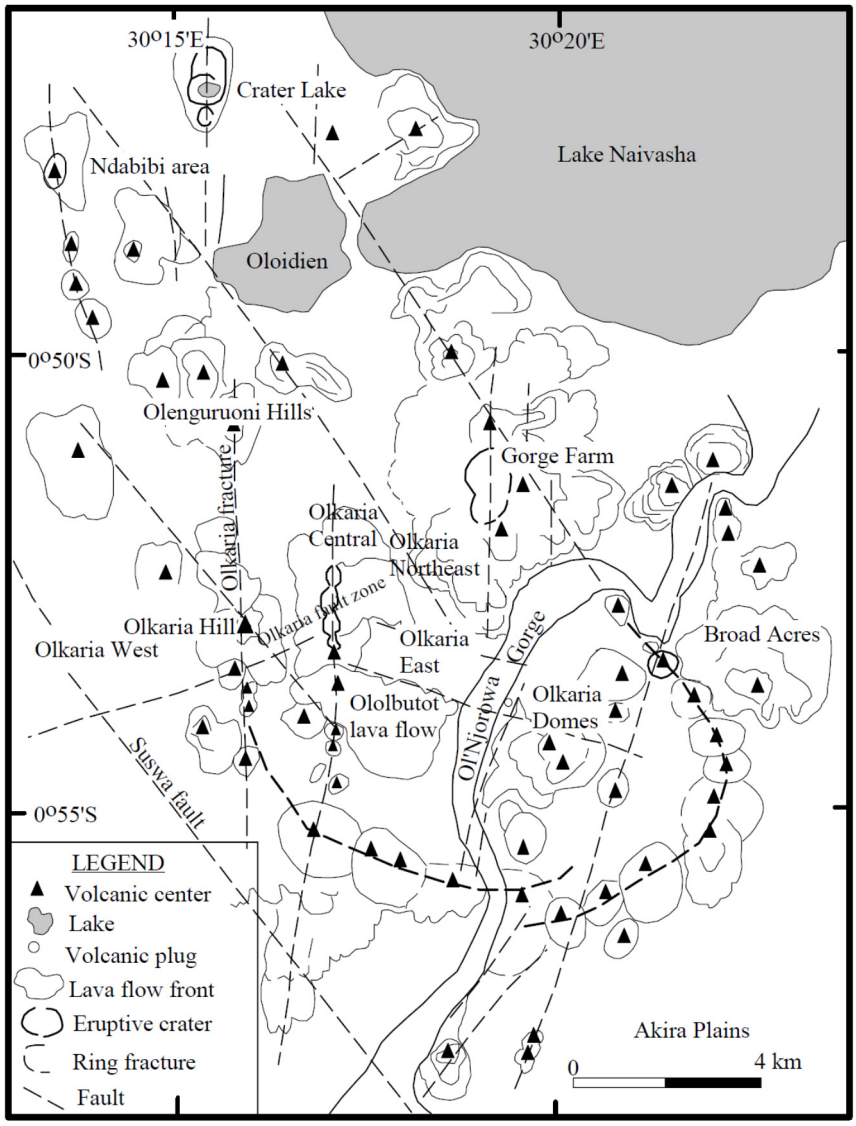

FIGURE 6: A tectonic structural map for the Greater Olkaria volcanic field (from Lagat, 2004)

The N-S and NNE-SSW trending faults are believed to be the youngest. They are associated with the most recent eruptions, e.g. Ololbutot comendite eruptions. The most prominent of these faults is the Ololbutot fault (Figure 6). The NW-SE and the WNW-ESE trending faults are the oldest faults whose formation was associated with a graben formation during the rift's development (Lagat, 2004). The largest of these faults is the Gorge Farm fault. The Gorge Farm fault bounds the geothermal field in the northeast, extending south to the Olkaria Domes area (Figure 6). Phreatomagmatic craters, which form a row where the extrapolated caldera rim trace passes, are located at the northern edge of the Olkaria Domes area. These are explosion craters and mark magmatic eruptions which occurred in a submerged country (Mungania, 1999). The development of the Ol'Njorowa gorge was initiated by faulting. The catastrophic outflow of Lake Naivasha at 20 ka BP during one of its high stands (Clarke et al., 1990) resulted in its current steep walls and depth. It separates the Domes field from the Olkaria East field (Figure 6).

2.4 Geophysical studies

Various geophysical studies have been carried out in the Greater Olkaria geothermal field since the early 1980s with varied levels of success. The study methods employed have been resistivity, seismology and gravity (Mwangi, 1984).

Resistivity surveys have been carried out in the Greater Olkaria geothermal field comprising over 100 soundings. Two methods were used:*Magnetotellurics (MT)* and *Transient Electromagnetic soundings (TEM)*. From the TEM inverted and interpreted data, the low-resistivity anomalies recorded are found to be controlled by linear structures with NE-SW and NW-SE trends (Mariita, 2009). From these data, it was interpreted that the geothermal resource was confined in an area that showed low resistivity, less than 15 Ωm, at an elevation of 1400 m a.s.l. (Figure 7). Relatively low resistivity was recorded around the Olkaria West field as compared to the Olkaria Northeast and East fields. This reflects the differences in the lithology at shallow depths (Omenda, 2000). The Olkaria West field is characterised by low pH value fluids which have high conductivity and extensive alteration due to thick tuff deposits near the surface with high permeability (Muchemi, 1999), the cause of low- resistivity anomalies. The relatively high resistivity in the East and Northeast fields partly arises from the fact that the reservoir in these two fields is hosted within flood trachytes. These trachytes have low susceptibility to alteration except along secondary structures, e.g. lithological boundaries and/or intrusions. These two fields are also characterised by high pH fluids which have low conductivity. The extremely low resistivity near Olkaria Hill in the Olkaria West field was postulated as being related to a heat source for that field (Mariita, 2009).

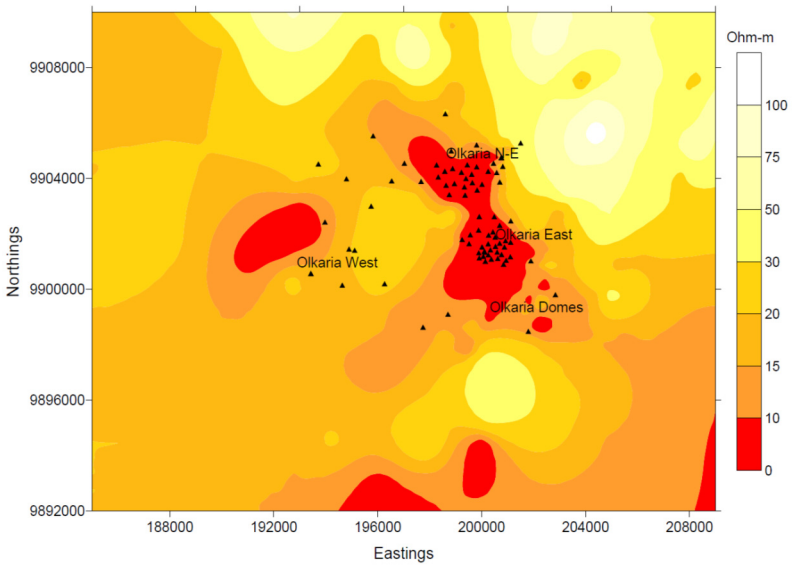

FIGURE 7: Resistivity distribution at 1400 m a.s.l. from TEM soundings in the Greater Olkaria geothermal field (Mariita, 2009)

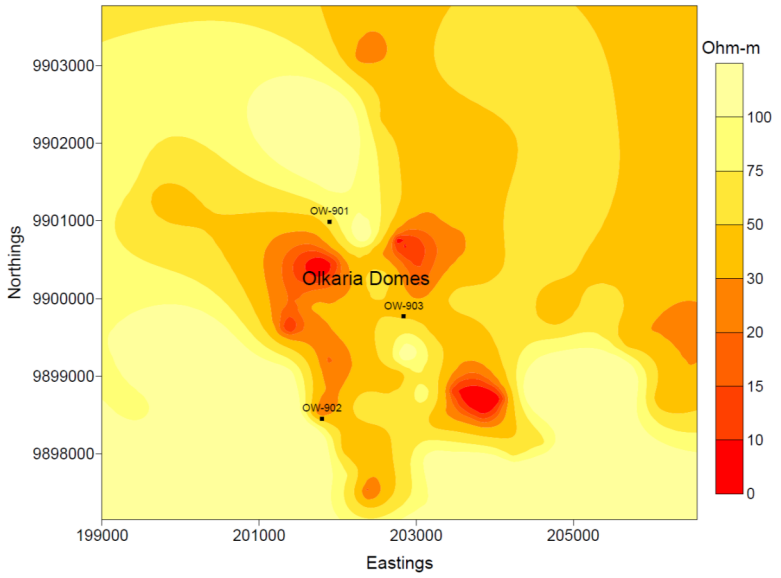

FIGURE 8: MT resistivity distribution at 1000 m a.s.l. at Olkaria-Domes geothermal field and its surrounding (Mariita, 2009)

The correlation between the MT data (Figure 8) and data from drilled wells in the whole of the Olkaria geothermal field has indicated that the low resistivity anomaly at 1000 m a.s.l. defines a geothermal system with temperatures above 240°C (Mariita, 2009). Some of the high resistivity anomalies observed in the West and East fields coincide with recharge areas associated with the N-S trending Ololbutot fault and the N-E trending Olkaria fault. These faults act as conduits for cold water flow from the Rift Valley

escarpments. Preliminary analysis of the MT data also suggests the presence of significantly enhanced conductivities below the Olkaria Domes area (Figure 8). However, no quantitative modelling of data has been done and the actual physical para-meters of the suggested zone of enhanced conductivity are not known (Mariita, 2009).

2.5 Petrochemistry of the Greater Olkaria volcanic complex rocks

Chemical analyses of the sub-surface and surface rocks from the Greater Olkaria volcanic complex show that the area is composed of rocks ranging from basaltic to rhyolite in composition (MacDonald et al., 1987, 2001; Omenda, 2000; Clarke et al., 1990). Based on the TAS classification scheme and CIPW norm calculations (Middlemost, 1989), the basalts are found to be close to silica saturation. The trachytes are mainly metaluminous while the rhyolites are mainly comendites (MacDonald, 1974). Lagat (2004) carried out chemical analyses on rock samples obtained from wells (OW-901, OW-902 and OW-903) drilled in the Domes area. He compared these analyses to the analyses carried out earlier in the Olkaria East and Northeast fields and surface samples from Broad Acres by MacDonald et al. (1987). The study shows that the rocks from Olkaria East, Northeast and the Broad Acres have a similar composition to the rocks extracted from wells OW-901, OW-902 and OW-903 in the Domes field. The chemical composition of these rock samples are shown in Figure 9.

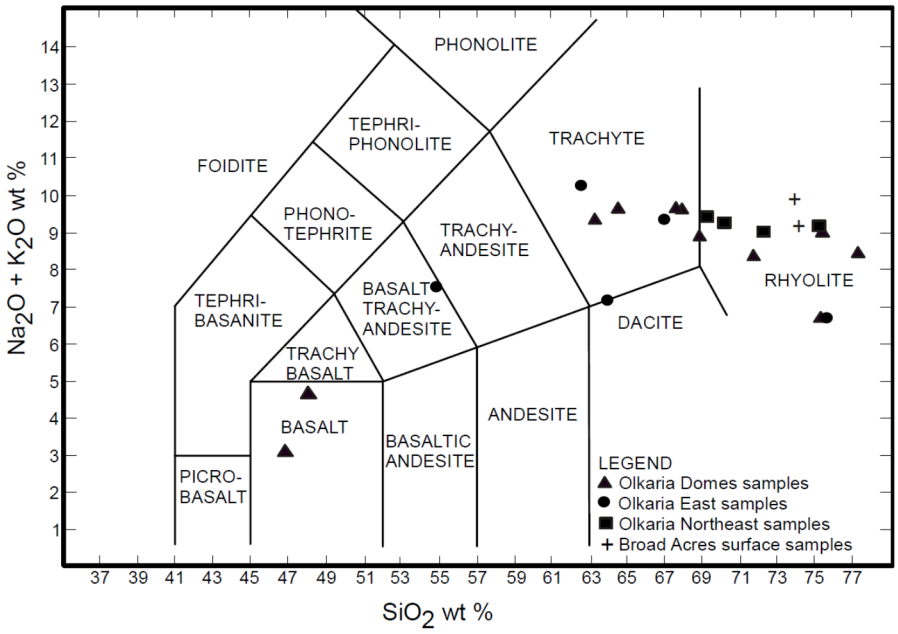

FIGURE 9: TAS diagram showing the chemical analysis of rock samples from the Greater Olkaria geothermal field and the Broad Acres area (Lagat, 2004)

3. SAMPLING AND ANALYTICAL METHODS

Sampling was done at the rig site during the drilling of the well. The drill cuttings were collected at 2 m intervals, except for depths where losses were encountered. The analysis of the samples was carried out at the rig site to enable the geologist and the drilling crew to understand the formations through which they were drilling, so that proper drilling procedures could be followed to avoid setbacks. Four main analytical methods were employed in the present study of the rock cutting samples from well OW-914A; they include: binocular microscope analysis, X-ray powder diffraction analysis, petrographic microscope analysis and fluid inclusion analysis.

3.1 Binocular microscope analysis

Binocular analysis of the rock cuttings was done at the rig with the use of a binocular microscope. This was done by first scooping each of the 2 m interval samples from the sample bag into a petri-dish and washing it in clean water. The sample was washed in clean water to remove impurities and dust in order to enhance visibility and reveal features such as finely disseminated sulphides, e.g. pyrite. The sample was mounted on the stage of a binocular microscope. The properties noted include the colour of the rock cuttings, texture and grain size, rock fabrics, vein fillings, porosity, mineralogy of the rock, alteration mineralogy, intensity of alteration and the rock type.

3.2 Petrographic microscope analysis

The petrographic microscope analysis was carried out in order to confirm the rock type(s) and alteration minerals as identified in the binocular analysis. It also exposed additional alteration minerals not observed by the binocular microscope and allowed the determination of the mineralogical evolution of the alteration minerals in the cuttings sample. Drill cuttings were selected from the lithological units encountered in well OW-914A and thin sections were prepared for petrographic analysis. A Leitz Wetzlar petrographic microscope was used for this analysis.

3.3 X-ray diffractometer analysis

This analysis was used to identify individual minerals, especially clays and zeolites. Samples were selected from all the lithological units identified by the binocular analysis. They were run in an X-ray diffractometer and printouts were made. A teaspoon full of cuttings was taken from the selected cuttings samples and placed in water in a test tube. This was shaken for four hours by arranging the test tubes in a shaker to dissolve the clays out of the drill cuttings. Drops of water from each of the dissolved drill cutting were each placed on a slide, which had been washed by acetone to enhance cohesion and adhesion of the water and the slide, where they settled for twelve hours before being taken for analysis. The clay samples were first run in the X-ray diffractometer and the peaks were recorded. The samples, still on the slides, were then placed in a glycol solution for 24 hours. They were subsequently run in the X-ray diffractometer and the peaks were recorded. The third run involved heating the clay samples to 550°C before running in the X-ray diffractometer. These completed the three clay analyses, which basically included the untreated sample analysis, the glycolated and heated sample analyses. The three peaks were recorded and from these we interpreted the type of clay in a particular cutting sample. The X-ray diffractometer analyses helped in defining the alteration zones with regard to clay minerals. These zones facilitated in deducing the alteration temperatures of various lithological units within the well's stratigraphy.

3.4 Fluid inclusion analysis

Fluid inclusion analysis involves the analysis of fluids trapped within vacuoles in mineral grains, which form either during crystal growth or healing of small fractures in the mineral grains. Upon heating, the vapour bubble, in the fluid, shrinks and only one phase of fluid will be present when the so-called homogenisation temperature (T_h) has been reached, which is close to the temperature conditions at the time when the fluid became trapped in the mineral. Polished thin sections of samples of quartz mineral grains were prepared for fluid inclusion analysis in this study.

4. BOREHOLE GEOLOGY

Well OW-914A is a deviated production well. It was deviated to the east with an inclination of 17.85° and azimuth N77.14°E. It was drilled to a total measured depth of 2996 m. It is a medium diameter hole. It is located in the Domes area and was drilled to gather steam for the Olkaria IV power plant, which is meant to generate 140 MWe. The well was also meant to confirm the resource to the east of well OW-914. Well OW-914A is located on the same pad as well OW-914 and has the following well coordinates: Easting E205295.97, Northing N9899794.05, with an elevation of 2015.76 m a.s.l. (Figure 10). The well is located on the eastern margins of the Domes geothermal field. Drilling of this well commenced on the 25th of June 2010, and 48 days passed until completion on the 11th of August 2010.

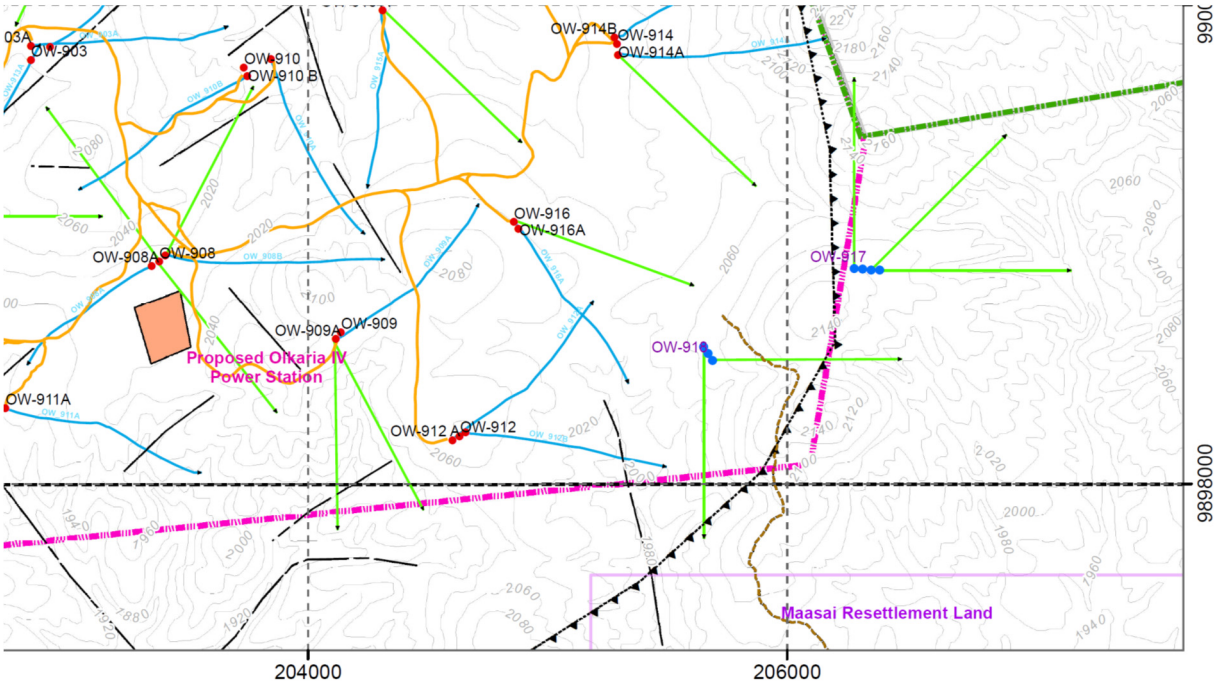

FIGURE 10: Location of well OW-914A within the Domes field of the Greater Olkaria geothermal field

Drilling progressed well, although losses of circulation returns were encountered at various depths. A summary of the casing depths and the well diameter is shown in Table 1. The drilling program was divided into four main phases as discussed below.

TABLE 1: Casing depths and drill bits of OW-914A

Drill rig	Drill bit (")	Maximum depth (m)	Casing depth (m)	Casing diameter (")
GWDC 188	26	63	63	20
GWDC 188	17½	307	290	13⅜
GWDC 188	12¼	867	866	9⅝
GWDC 188	8½	2996	2990	7

4.1 First phase (surface casing)

Drilling of a 26″ surface hole commenced at 10 m from the surface downwards ending at 63 m. The first stage was drilled with the use of mud and good circulation returns were experienced. At 63 m, the 20″ surface casing was run in the hole. Primary cementing was conducted followed by one backfill after

the cement failed to return to the surface with the primary cement job. About 20.34 tonnes of cement were used to anchor the casing. This stage was completed after 3 days (Figure 11).

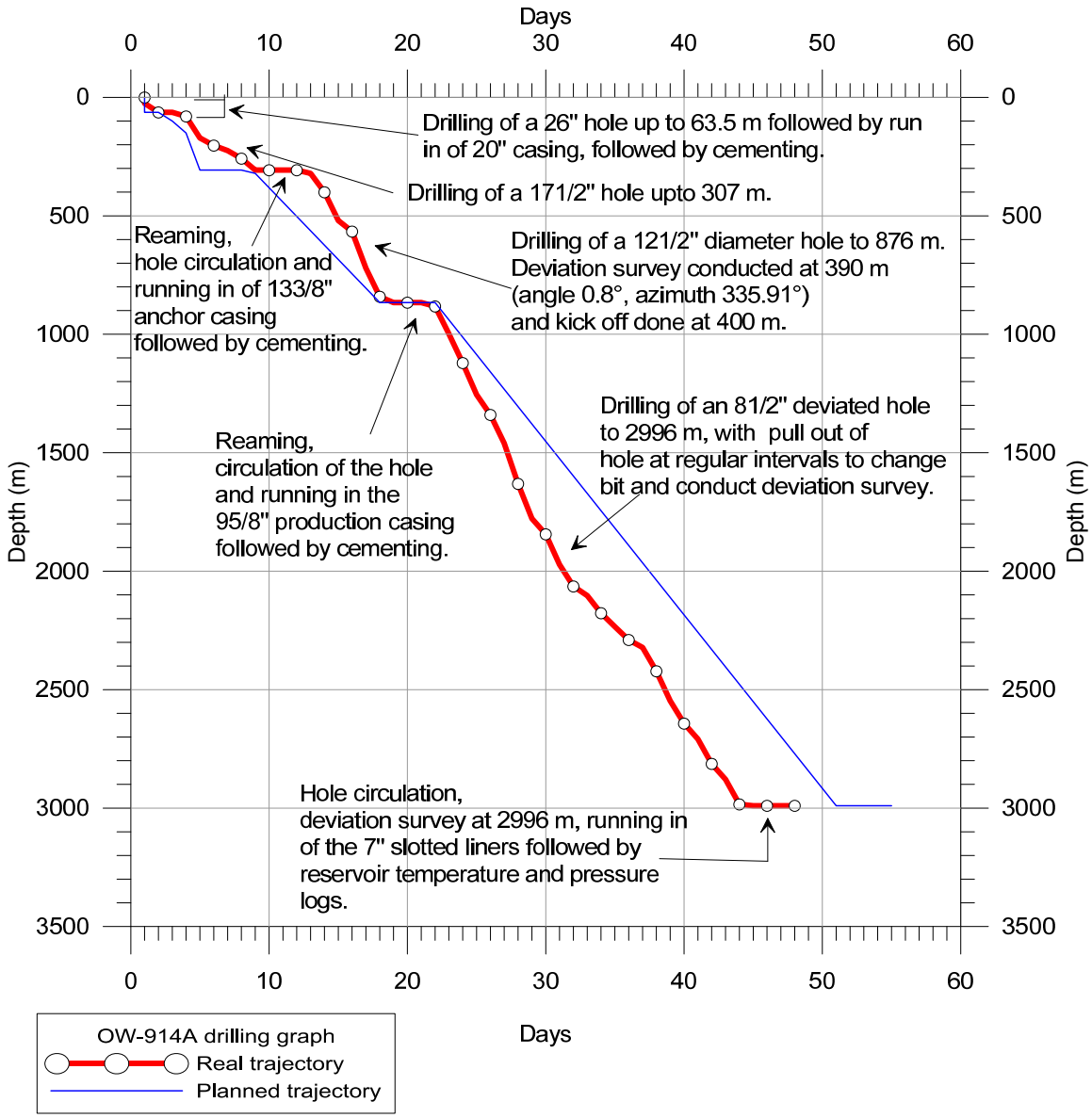

FIGURE 11: The drilling progress curve for OW-914A

4.2 Second phase (anchor casing)

This phase involved drilling a 17½″ diameter hole; this section was drilled with the use of water as the circulation fluid. Good circulation returns were experienced until 89 m depth. Drilling continued with water but total loss of returns was recorded from 89 to 211 m depth. At 211 m depth, the drill bit and the BHA setup were changed and drilling continued with aerated water and foam from 211 down to 225 m with partial circulation returns being experienced. From 225 down to 307 m, water was once again employed. Full circulation returns were obtained. At this depth, the hole was reamed and circulated with aerated water and foam to clean it prior to casing and cementing. The anchor casing, 13⅜″, was run in at this depth with cement returning to the surface after the 4th backfill, with a total of 61.13 tonnes of cement being used. This stage was completed after 9 days on the 6th of July 2010.

4.3 Third phase (production casing)

After a successful wellhead assembly and pressure test of the blind ram, drilling of the 12¼″ diameter hole for the production casing resumed with a similar diameter bit. The drilling proceeded with water with full returns until 400 m depth. The first deviation survey was conducted at 390 m depth and after that the kick off was initiated at 400 m. The rate of build-up was 3° per 30 m (100 ft). Drilling continued with water down to 567 m with good circulation returns. From 567 m depth, drilling continued with aerated water and foam until the casing depth was reached at 867.19 m depth (Figure 11). The hole was rinsed and reamed and after that the 9⅝″ production casing was run in the hole. Cementing was successfully completed with one backfill and a total of 43.56 tonnes of cement was used. This stage took 9 days to complete. It was completed on the 15th of July 2010.

4.4 Fourth phase (production section for slotted liners)

Drilling of the 8½" production section commenced on the 16th of July 2010 with water as the circulation fluid from 867.19 m to 2996 m depth. There were full returns from 867.19 to 2296.8 m depth. Deviation surveys were carried out at regular intervals until 2296.8 m depth. Between 2296.8 and 2422 m, there was total circulation loss. Returns were received on the surface between 2422 and 2643.55 m as drilling continued with the use of aerated water and foam. Loss of returns was experienced from 2643.55 to 2709 m depth. From 2709 to 2996 m, drilling with aerated water and foam continued with good circulation returns. After the final depth had been reached at 2996 m, the hole was circulated, and drill rods were returned in the hole for wiper tripping. A deviation survey was conducted at 2990 m depth showing that the inclination of the well was 17.85° and the azimuth N77.14°E, which was within the target range. The 7″ slotted liners were run in the well, followed by temperature and pressure well logging before breaking the stands to singles and releasing the rig on the 11th August 2010 at 16:30 hrs. The well was completed within the stipulated time, as shown by the drilling progress in Figure 11.

4.5 Stratigraphy

The litho-stratigraphy of well OW-914A is mainly comprised of five types of rock units. These are: pyroclastics, tuff, rhyolite, basalt and trachyte. Scarce rhyolitic and basaltic intrusions also occur intercalating with the tuffs, basalts and trachytes. The classification of these lithological units was based on the texture of the drill cuttings and their mineralogy (the presence of quartz as a primary mineral or the absence of it, the abundance of feldspars, mafic minerals, and the abundance of lithic groundmass and/or lithic fragments). This classification was mainly based on binocular and petrographic microscope observations. A detailed description of the lithological units seen in well OW-914A is outlined in Appendix I. Figure 12 shows the lithological units seen in this well together with circulation fluid temperatures and the drilling parameters. Below is a summary of the lithological units in well OW-914A.

The *pyroclastics* are brown to yellowish in colour. The rocks consist of fragments of rhyolite, tuff and trachyte. The matrix is mainly made of ash material, relatively fresh volcanic glass, palagonite, pumice, feldspars, quartz and amphiboles. The pyroclastics form the uppermost 90 m and are also observed at 232-290 m depth in well OW-914A.

*Rhyolite***.** Two types of rhyolites were encountered. The first type ranges from fine grained to medium grained, porphyritic with pyroxenes and quartz phenocrysts. It is mainly whitish to brownish grey in colour. In the petrographic microscope it appears glassier with aegerine-augite, quartz and a few sanidine phenocrysts distributed within a ground mass dominated by finely-grained quartz mineral grains. This type shows a spherulitic texture with laths of sanidine and quartz crystals radiating from a central point. The first type occurs between 100 and 312 m. The second type of rhyolite is fine to medium grained, mainly aphyric brownish grey in colour with sanidine, pyroxenes and fine-grained

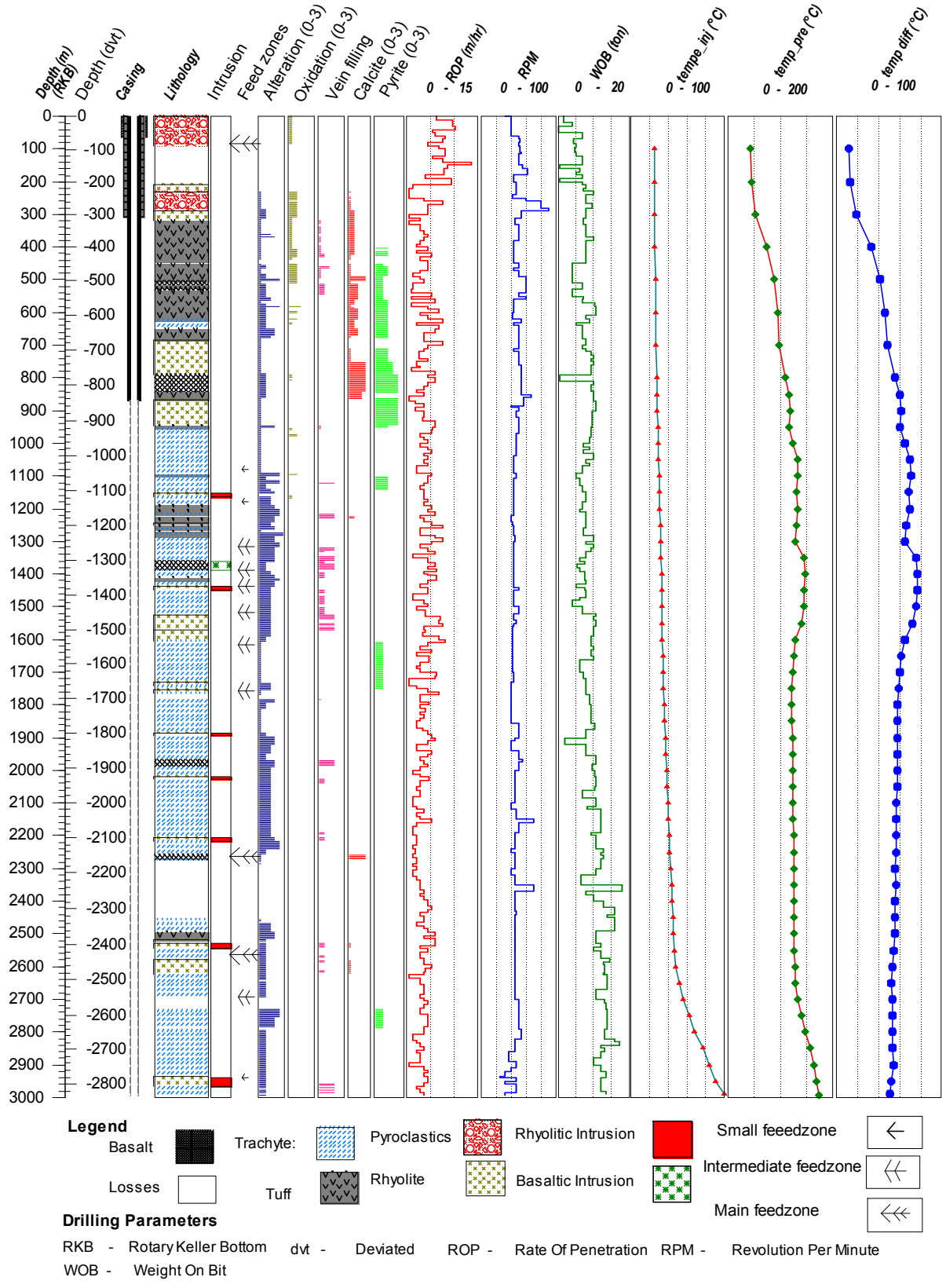

FIGURE 12: Lithological units, circulation fluid temperatures and drilling parameters for well OW-914A

quartz grains forming the ground mass. This second type occurs from 684 to 2544 m depth, intercalating with other lithological units as shown in Appendix I.

Tuff is greenish, brownish grey to white in colour. The tuff occurs in three types: glassy (vitric) tuff, lithic (fragmental) tuff and welded tuff. The glassy tuff is mainly non-crystalline and highly vesicular. It only occurs at shallow levels from 312 down to 408 m as a single layer. The lithic tuff consists of lithic fragments of lava with crystals embedded in a glassy groundmass. The fragments include feldspars, quartz, aegerine-augite and amphiboles. The welded tuff is characterised by finely grained ash material in which larger shards of volcanic glass and pumice fragments are discerned. Under the petrographic microscope, these fragments appear deformed with the glass fragments showing a fiamme texture, typical of the straining they were subjected to during the welding process. The lithic and welded tuffs occur intercalating with other lithological units all the way down to the bottom of the well. The tuff generally occurs from 318 down to 682 m depth as a thick stratum with intercalations of basalt and trachyte rocks. Below 682 m the tuffs mainly occur as intercalations with a range in thickness from 4 to 26 m.

Trachyte occurs from 624 m all the way to the bottom of the well. It is the dominant rock type at depth. It occurs with intercalations of other rock units. When fresh, the trachyte appears grey and quite massive with sanidine and pyroxene phenocrysts, whereas altered trachyte appears light grey to brownish, attributed to the oxidation process, caused by hydrothermal alteration. The trachyte is fine to medium grained and highly porphyritic. It has phenocrysts of sanidine, clinopyroxenes, riebeckite and the discrete minute crystals of Fe-Ti oxides. Sanidine is the dominant mineral, easily distinguished under petrographic microscope by its Carlsbad twinning. Two types of trachytes occur in the well. The first type lacks the flow texture and has relatively less clinopyroxenes. This type mainly occurred from the surface down to 1200 m depth. The second type has a characteristic flow texture with the mineral grains showing elongation in a particular direction, an appearance observed in both binocular and petrographic microscope. It has abundant sanidine and a few microcline grain phenocrysts. This type was mainly observed below 1200 m depth.

Basalt occurs sporadically between 510 and 2274 m but also in between other lithological units. It is fine to medium grained, highly porphyritic and dark grey to greenish in colour. It has phenocrysts of plagioclase and clinopyroxene. In petrographic microscope observations, it has abundant plagioclase and clinopyroxene phenocrysts. The plagioclase occurs in elongated laths. The clinopyroxene phenocrysts are intermittent and subhedral to euhedral in shape. Olivine is absent in the basalt in this well because of alteration but the shape and outline of some of the clay fillings show that they have replaced olivine.

A *basaltic intrusion* was encountered between 1364 and 1388 m depth. The intrusion is fine grained and dark grey in colour. It shows abundant pyroxene. It has plagioclase feldspars and pyroxene phenocrysts. The rock appears relatively fresh with chilled margins and the rock units bordering the intrusion show extensive alteration with the deposition of abundant high-temperature actinolite.

Rhyolitic intrusions occur from 1154 m, appearing at various intervals down to 2966 m (Figure 12). They are whitish in colour, fine-grained and appear relatively fresh. Micro-phenocrysts of quartz and aegerine-augite occur within the groundmass. They have chilled margins, and shows high oxidation at the contact zone, an indication of the heating effect along the boundary with the host rock. The intrusions had similar characteristics, an indication that they may belong to a similar intrusive phase, which resulted in numerous intrusions cutting across the lithology in this area. This intrusive phase may be the same phase that formed the dome-like structures of rhyolitic composition, which are aligned along the loci of the hypothesised collapsed caldera rim. Further analyses on the composition of these intrusions and the dome-like structures are needed to ascertain this.

5. HYDROTHERMAL ALTERATION AND TEMPERATURE DISTRIBUTION

Hydrothermal alteration is the change in mineralogy, texture and chemistry of the rock as a result of the interaction of the rock with hot fluids, called "hydrothermal fluids" (Browne, 1978). Hydrothermal fluids are water and / or steam (including gases) that can be found several hundreds of meters to several kilometres in fractured or porous rocks below the earth's surface. These fluids vary in temperature from 32°C to about 400°C. Hydrothermal fluids carry dissolved solids in solution, either from a nearby igneous source or from leaching out of country rocks. As the fluids interact with the rock, the dissolved ions are either added to the ions in the primary rock forming minerals, or react with ions in the primary rock, extracting them from the rock. The fluids may also deposit some of the dissolved solids in voids and vesicles according to the temperature conditions at the point of deposition. This results in the formation of secondary minerals. The secondary minerals are either stable or metastable in the existing hydrothermal alteration environment under which they form (Browne, 1978).

In a geothermal environment, the rate and intensity of hydrothermal alteration is dependent on six main factors: temperature; permeability (influences the rate of percolation of the fluids and their interaction with the rock); pressure (not always directly, but controls the depth at which water boils and also brings about changes in terms of mineral phase equilibrium (Gebrehiwot, 2010)); fluid composition; duration of exposure of the primary rock forming minerals to the hydrothermal fluids; and the mineral composition of the primary rock being subjected to alteration (Browne, 1978). During hydrothermal alteration, some of the rocks undergo oxidation or reduction (bleaching), revealing conspicuous changes to their original colour. Studies have been done in the past in an attempt to correlate the alteration minerals with the formation temperature. Most of these minerals are deposited at specific temperature conditions, for example, epidote, in a typical high-temperature geothermal field, is deposited at a minimum temperature of about 240°C. The temperature conditions during the deposition of the alteration minerals, under which the alteration mineral is stable or metastable, may correlate to formation temperature if the system is in equilibrium.

5.1 Hydrothermal alteration minerals of well OW-914A

The alteration minerals in the Domes geothermal field appear either as deposition minerals or replacement minerals. Deposition minerals appear deposited in vesicles, fractures and vugs, into which they precipitated from the hot hydrothermal fluids, whereas replacement minerals replace the primary rock-forming minerals.

The main alteration minerals found in well OW-914A were albite, adularia, amphibole (actinolite), calcite, chalcedony, epidote, fluorite, oxides (Fe-Ti oxides), garnet, clays (illite and chlorite), sulphides (pyrite), titanite (sphene), prehnite, wollastonite, quartz (secondary) and low and high-temperature zeolites (scolecite/mesolite and wairakite, respectively). The distribution of the alteration minerals in OW-914A is shown in Figure 13; below is a description of these minerals.

Scolecite and mesolite were first observed at 200 m depth and disappeared at 240 m depth. These are low-temperature minerals stable between 60 and 100°C. They occur together, filling vesicles. In some of the samples, they appeared in association with opal and chalcedony. The scolecite crystals appeared colourless and flattened while the mesolite crystals appeared in spikes and red in colour. The scolecite and mesolite crystals radiate from a single point growing in fibrous aggregates.

Calcite is distributed from the near-surface depth all the way down the well, with its first appearance being noted at 350 m depth. It appeared white in colour and in varying abundance, with a relatively high abundance being noted in the shallow level tuff from near-surface to 800 m, and the basalts at 506, 524 and 792 m depth. In OW-914A, calcite replaces sanidine, volcanic glass, pyroxenes and plagioclase feldspars and also directly precipitates in fractures and vesicles. Its abundance in the basalt is attributed to the calcium oxide-rich plagioclase minerals in the Olkaria basalt, as observed by MacDonald et al.

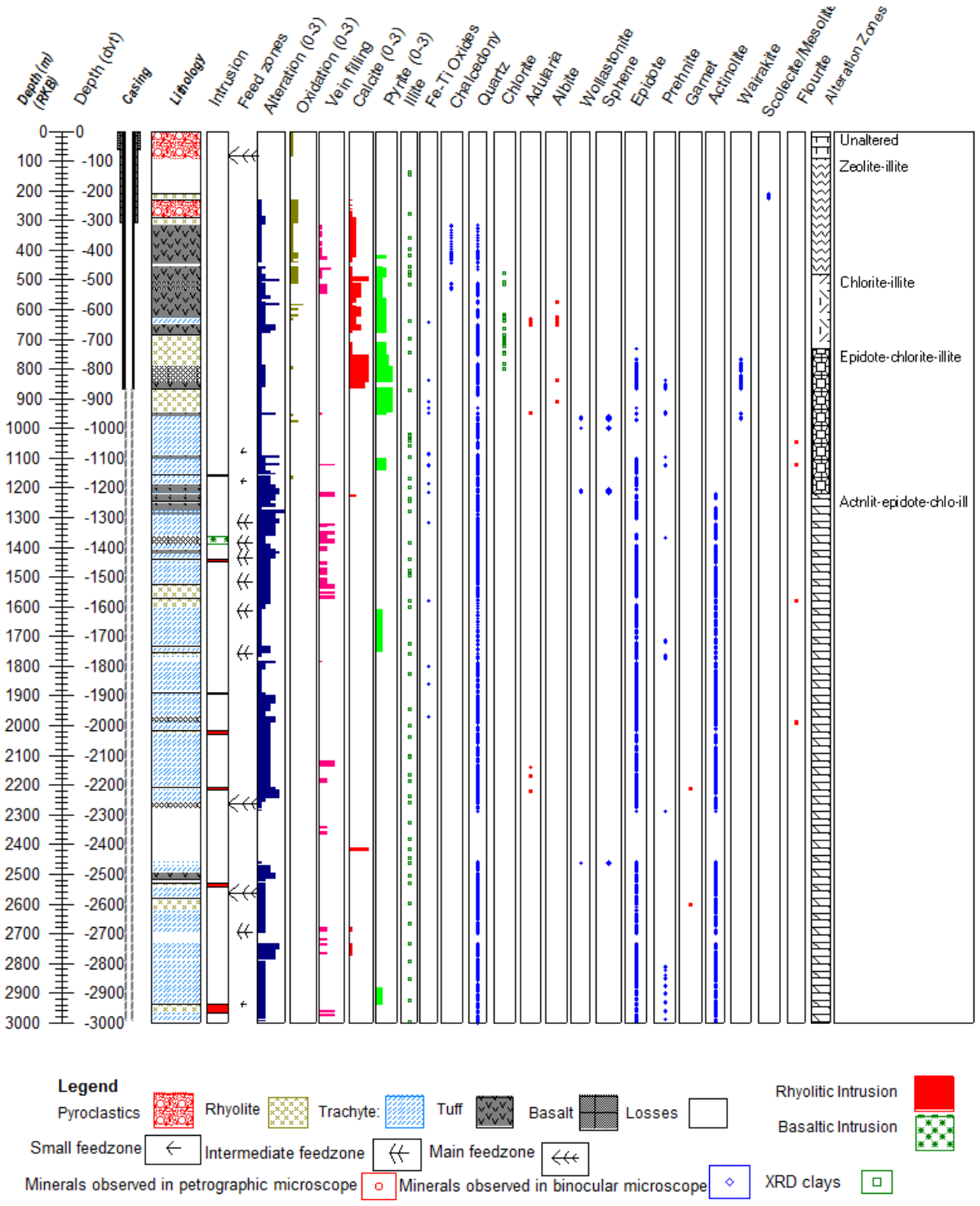

FIGURE 13: Lithology, distribution of alteration minerals and alteration zones in OW-914A

(1987). The tuff at the shallow level is highly vesicular and, therefore, highly permeable, allowing for precipitation of dissolved calcite from the hydrothermal fluids. Platy calcite rarely occurred in the samples but was observed under petrographic microscope as thin lamella crystals appearing in layers. Under the petrographic microscope, calcite was identified by its rhomboid cleavages, high birefringence and change of relief with rotation. Calcite precipitates from water solutions at temperatures below 280°C. The formation of platy calcite can be linked to boiling conditions in a geothermal system (Stuart and Browne, 2000). The presence of calcite is determined by the use of dilute hydrochloric acid (HCl); on the addition of HCl in the cuttings sample, effervescence occurred if it contained calcite.

Pyrite appears as brass yellow, well developed, cubic crystals. It is mainly disseminated in the ground-mass of the rock in which it appears. It first appeared at 404 m down to the bottom of the well. It occurred in varying amounts with depth but was in relatively large abundance in the shallow level tuff, from the near-surface to 800 m depth. It appeared opaque in the petrographic microscope with its characteristic cubic shape. The presence of pyrite indicates good permeability in the rocks.

Chalcedony first appeared at 102 m and was last seen at 430 m depth. It appears in a spherical growth, white to pale blue in colour and growing in vesicles. In some samples, it appeared overgrown with quartz. This is a low-temperature alteration mineral, stable between 100 and 180°C.

Opal appeared in a milky white colour at 102 m and 150 m depth. It appeared in an almost amorphous shape, filling in cavities. It is a low-temperature mineral, indicating temperatures below 100°C.

Quartz mainly appears as a precipitation mineral filling vesicles and fractures. In some of the fractures, it had formed quartz veins. It also appeared as an alteration product of chalcedony. In the binocular microscope, it appeared euhedral to anhedral, transparent mineral grains. Euhedral grains appear as hexagonal prismatic crystals ending in a six-faced slanting apex analogous to a hexagonal pyramid. Some of the quartz was noted growing in clustered, small euhedral crystals while others grew individually. Quartz is found growing in association with wairakite, epidote, calcite and wollastonite. In thin sections, it is easily identified by its lack of cleavage and the undulating extinction. It is colourless with slightly higher relief than the resin. The appearance of quartz indicates a formation temperature of about 180°C. Quartz was first noted in this well at 318 m depth and was seen down to the bottom of the well.

Wairakite is a scarce mineral in this well. It was first observed at 762 m depth and was seen sporadically, disappearing at 968 m depth. It is generally found filling the open spaces in vesicles and fractures. It grows in association with quartz and epidote. The crystals are transparent in the petrographic microscope, have clear crystal faces and are mainly found growing in clusters. Wairakite is stable at about 200°C and above.

Epidote was first noted at 732 m. It occurred down to the bottom of the well. It occurs in association with quartz, prehnite, wollastonite and actinolite. It is greenish to yellow-green in colour. It grows in vesicles and also replaces plagioclase and pyroxene. Epidote shows various crystal forms from euhedral to anhedral. The euhedral crystals are mostly within vesicles, primarily as a depositional product. They are tabular, and grow in a radiating manner. The anhedral crystals mainly occur as a replacement of plagioclase. In thin sections, it is yellow green with high interference colours and parallel extinction. It is a high-temperature mineral stable at about 240°C and above.

Prehnite was first observed at 836 m and occurred down to the bottom depth of the well. It grows in association with epidote and wollastonite. It appears yellowish-white and in small radiating grains which form lamellar aggregates. In other cutting samples, the crystals formed box-like platy aggregates in fan-shaped clusters. The crystals were observed filling vesicles. In thin section, it forms bow-tie structures and shows high interference colours. It is a high-temperature mineral, which forms at about 230-240°C at minimum.

Wollastonite was first noted at 856 m and occurred intermittently down to the bottom of the well. It is whitish in colour, fibrous, with needle-like crystals growing in aggregates. It was mainly observed deposited in vesicles and in veinlets. In thin section, it forms fibrous, colourless and translucent crystals, which show low, first order grey interference colours. It starts to form at 270°C and grows in association with prehnite, epidote and actinolite.

Actinolite was first noted at 1218 m depth and occurred with increasing abundance down to the bottom of the well. It grows in association with epidote and wollastonite, where they are found filling in vesicles. It has very slender crystals: highly fibrous, greenish to whitish in colour growing in radiating

aggregates. It was observed growing in vesicles. With increasing depth, actinolite starts to replace pyroxenes. This was noted at 2200 m depth. In the thin section, it appears as pale green to colourless long prismatic crystals; in other instances, it appears as highly fibrous crystal aggregates. It shows 3rd order interference colours and has a high relief. It forms at about 280-290°C.

Garnet is a high-temperature mineral that starts to form at about 300°C. Garnet is a scarce mineral in this well. It was noted at 2208 m depth under the petrographic microscope, in association with a rhyolitic intrusion noted at 2206 m depth. It is an isotropic mineral. It appears in dodecahedral crystals with a rough surface. This mineral was found growing in granular and compact form.

Fluorite is a rare mineral in this well, being noted at 1046 m depth with intermittent occurrence down to 1580 m depth. It was noted under the petrographic microscope. It is cubic and thus, isotropic, and has a perfect cleavage. The crystals are euhedral, showing square outlines. Fluorite has low relief.

Adularia occurs mainly when replacing sanidine feldspar but is occasionally deposited in veins. It occurred below 500 m depth and disappeared at 2640 m depth. It forms euhedral to anhedral crystals that are diamond shaped. It forms above about 190°C.

Albite is an alteration mineral of sanidine feldspar. It is cloudy white in colour with anhedral to euhedral crystals. It has low refractive indices almost equal to the resin. Some of the crystals occurred in lath-shaped sections. The original plagioclase twinning is replaced on alteration by the cloudy nature of albite. It first appeared at 574 m depth and disappeared at 1000 m depth. It forms above about 180°C.

Sphene was first observed at 850 m depth and is present down to about 2500 m depth of the well. It appears colourless with an acute rhombic cross-section. It has high-order interference colours. It was observed disseminated in the rock matrix replacing FeTi-oxides.

Oxides are formed by the release or addition of ions out of primary or secondary minerals. Many types of oxides are formed through oxidation, depending on the metal cations present. The main oxides encountered in well OW-914A were FeTi-oxides. The FeTi-oxides were encountered at near surface depth disappearing with depth. Hematite and rutile were observed. The hematite is reddish brown to steel-grey in colour and was observed in the binocular microscope at 620 m depth. Rutile, a Ti-oxide, was observed in the petrographic microscope at 1318 m and disappeared at 2050 m depth. It has a red brown colour and occurs in small prismatic crystals with high-order interference colours.

Clay minerals are alteration products of volcanic glass, olivine, plagioclase, sanidine and pyroxene. The clay minerals are important hydrothermal alteration products. Different clay types cover the temperature stability field relevant for geothermal systems. The clays encountered in well OW-914A were observed to fill vesicles and veins and also occurred as alteration products of the primary minerals. Both fine-grained clays (illite and chlorite) and coarse-grained chlorite were observed. This was mainly determined by the use of the X-ray powder diffraction analysis. Different clays showed different and unique peaks. The clays encountered are discussed below.

Illite: This appears greenish, brownish to whitish in colour under the binocular microscope. It appears green to brown under the petrographic microscope. It was observed as a vesicular lining and as an alteration product of sanidine and volcanic glass. It forms at 200°C and above. Under XRD analysis, its first appearance was at 278 m and it was prevalent down to the bottom of the well at 2996 m. It showed peaks between 9 and 10 Å in untreated, glycolated and heated samples (Appendix II).

Chlorite: It appears pale green in both binocular and petrographic microscope. It is associated with illite. It occurred in a paragenetic sequence in some of the samples. It seems to have deposited after the fine-grained illite and before epidote in samples where they filled vesicles and veins together. Chlorite is fine- to coarse-grained and non-pleochroic. There are two types of chlorite, based on XRD analysis: - stable and unstable. The unstable chlorite appears pleochroic in the petrographic analysis with more

dynamic colours, almost resembling the mixed layer clays, while the stable chlorite is green and weakly pleochroic, pale green in colour and mainly coarse-grained. Chlorite first appeared at 480 m depth and was seen down to 762 m depth, as indicated by peaks at 7 and 14 Å for untreated and glycolated samples, while after heat treatment, the 7 Å peak collapsed for unstable chlorite; stable peaks were observed in all three treatments for stable chlorite (Appendix II). Chlorite has a minimum crystallisation temperature of about 200°C.

5.2 Alteration of primary minerals

The primary minerals are rock forming minerals that were formed during crystallisation and / or re-crystallisation of the magma as it cooled. These minerals are unstable in hydrothermal conditions. These minerals, when subjected to hydrothermal conditions, are replaced by secondary minerals which are stable at the new temperature and pressure environment (Browne, 1978). The primary minerals in the rocks penetrated by well OW-914A are characterised by an abundance of volcanic glass, plagioclase, pyroxene, olivine, amphiboles, sanidine, microcline and Fe-Ti oxides (primary). These minerals, where subjected to alteration, have been replaced by various secondary minerals (Table 2). A summary of the primary minerals found in well OW-914A is given below.

TABLE 2: Primary minerals, order of replacement and alteration products of well OW-914A (modified from Browne, 1984)

	Primary minerals	**Alteration products**
Most susceptible	Volcanic glass	Zeolites, clays, quartz, calcite
	Olivine	Chlorite, actinolite, clay
↓	Pyroxenes, amphiboles	Chlorite, illite, quartz, pyrite, calcite
	Plagioclase	Calcite, albite, quartz, epidote, sphene
Least susceptible	Sanidine, microcline	Adularia, chlorite, illite, calcite
	Fe-Ti oxides	Pyrite, sphene, hematite

Volcanic glass and amorphous silica are the dominant phases in the near-surface rocks. They were mainly observed in the tuff and rhyolite rocks. Glass forms when magma solidifies without getting enough time to crystallise, even though it is not classified as a primary mineral. Perlitic texture, characteristic of volcanic glass, was observed in its alteration products. Volcanic glass alters to clays, zeolites, quartz and calcite. Its alteration was first noted at 20 m with the formation of palagonite.

Olivine is rare in this well. Its presence as a primary mineral was mainly deduced from the retained olivine shape in the alteration products, especially clays. This was only noted in the basalt units. It alters to chlorite, actinolite and hematite. This mineral starts altering at 506 m depth in the well.

Pyroxene, amphiboles: These minerals are relatively abundant in some of the cutting samples. They appear to have undergone relatively little alteration in some of the samples since they were clearly identified in both the petrographic and binocular analysis. The aegerine-augite pyroxenes were noted in this well. Hornblende was also noted in this well. Their alteration products in this well include chlorite, illite, quartz, hornblende, pyrite and calcite. These minerals start altering below 250 m depth.

Plagioclase is a relatively dominant feldspar in the cuttings of this well. They form the phenocrysts in basalt. They alter to form calcite, albite, adularia, quartz, illite, epidote, and sphene. Its alteration was seen below 250 m depth.

Fe-Ti oxides: Magnetite and primary rutile are the main Fe-Ti oxides in this well. When altered, they form hematite, pyrite and sphene. The Ti-rich oxides, e.g. rutile, showed resistance to alteration. They show minor or no alteration in the petrographic microscope. The iron oxides are altered at surface conditions from magnetite to hematite. Their alteration was first noted at 50 m depth.

Sanidine, and microcline: Sanidine is the dominant phenocryst in the trachytes. Microcline was observed in minute quantities and mainly in the trachytes. They show high intensity of alteration at the highest temperature conditions. The alteration product is adularia, calcite, illite and chlorite. They were noted to alter to adularia from 500 m depth and to albite from 574 m down to the bottom of the well.

5.3 Alteration mineral zonation

The distribution of alteration minerals in a well gives information about the formation temperature of the well at the time the alteration minerals were formed. From the analysis of alteration minerals, information as to whether the geothermal system has been cooling or heating up can be obtained. This is achieved by comparing the temperatures during the formation of the alteration minerals, to the measured formation temperatures from the well. Most of the minerals that provide information on formation temperature are those that contain the OH^- or nH_2O in their structures (with a few exceptions) (Brown, 1978). These include zeolites, clays, epidote, prehnite, wollastonite, garnets and amphiboles. Based on hydrothermal mineral assemblages identified in well OW-914A, five alteration mineral zones were identified (Figure 13). Each zone marks the beginning of a new assemblage, marked by the first appearance of the index mineral that appears first in the name of that zone. These are discussed below.

Unaltered zone (0-90 m)
This zone is unaltered with most of the primary minerals having been retained in the rock. The unaltered glass was conspicuous in the thin sections. The main rock unit in this zone was the pyroclastics. Alteration that could be related to hydrothermal activity was not observed in this zone. Alteration minerals observed were hematite and palagonite, which form under near-surface conditions when cold groundwater percolates through the rock.

Zeolites-illite zone (90-480 m)
This zone was noted between 90 and 480 m depth. It is characterised by the presence of zeolites, calcite, chalcedony, pyrite and illite. The first appearance of the zeolites marks the upper boundary of this zone. The alteration temperatures in this zone range between 60 and 200°C.

Chlorite-illite zone (480-732 m)
This zone marks the first appearance of chlorite. Illite still persists throughout this zone. Another mineral observed in this zone was secondary quartz. These minerals form at relatively high temperatures of about 200°C and above.

Epidote-chlorite-illite zone (732-1218 m)
This zone indicates a temperature range of about 240-280°C. It is marked by the first appearance of epidote at 732 m. This zone extends down to 1218 m. Quartz, epidote, illite, wairakite and prehnite are the alteration minerals observed in this zone. Chlorite in this zone occurs down to 762 m depth.

Actinolite-epidote-chlorite-illite zone (1218-2996 m)
The upper boundary of this zone is marked by the first appearance of actinolite, and it is characterised by its abundance. Actinolite was noted between 1218 m to the bottom of the well at 2996 m. The alteration minerals found in this zone include quartz, illite, prehnite, epidote, wollastonite, actinolite and garnet. This zone indicates temperature of about 280°C and above.

5.4 Vein and vesicle fillings

Vein fillings are fractures that are filled with minerals deposited from hydrothermal fluids. The fractures are developed when the rock is subjected to stress and strain. Vesicles are small cavities in igneous rocks, mostly volcanic rocks, formed mainly by expansion of gas or steam bubbles that formed at the time the rock solidified. The presence of veins and vesicles in a rock enhances its permeability and

porosity but also acts as sites for the deposition of secondary minerals. Hydrothermal alteration minerals are deposited in fractures and vesicles to form vein fillings and amygdales. These alteration mineral deposits, which are used as geothermometers, enable the reconstruction of the paleo-thermal history of a geothermal system. Porosity is simply the measure of the void space within a rock, while permeability is a measure of the capacity of the rock to transmit fluid. Fractures provide secondary permeability to the rock but vesicles provide primary permeability and porosity.

Near the surface in well OW-914A, the vesicles were mainly filled with calcite, clays and zeolites. At greater depths, 700 m and below, there were both veins and vesicles. The vesicles were mainly filled with quartz, epidote, wairakite, prehnite, wollastonite, actinolite, clays and calcite. The vein fillings identified under both the petrographic and binocular microscopes were epidote, quartz and calcite. In some of the vesicles and fractures, minerals were deposited in layers, providing important information about the paragenetic sequence in these structures.

5.5 Mineral deposition sequences and paragenesis

Variations in the pressure, temperature and chemical constituents of a hydrothermal solution will result in the precipitation of different alteration minerals at different times. Paragenesis is the time-successive order of deposition of a group of minerals in a fracture or a vesicle. By studying depositional sequences, the equilibrium phases that existed at different times of the geothermal system can be deduced. This enables the thermal history and the relative time scale of alteration minerals within a geothermal system to be explored.

The depositional sequences noted in OW-914A included clay minerals, quartz, calcite and some high-temperature minerals. Table 3 summarises the sequences observed using both petrographic analysis and binocular analysis. The sequences involving the clays indicate the evolution of the system from lower to higher temperatures. At shallow depth in the well, a layer of coarse-grained clays was deposited after the fine-grained clays. Coarse-grained clays are deposited at a higher temperature than the fine-grained clays because of the coarse-grained clays´ temperature dependent structure (Franzson, 2012). A quartz vein is also observed deposited after calcite in the middle depth of the well, at 1118 m depth, an indication of thermal evolution from low to high temperatures. Epidote was deposited before wollastonite and / or actinolite at greater depths in the well, consistent with thermal evolution from lower temperature to higher temperature.

TABLE 3: Depositional sequences of hydrothermal alteration minerals at various depths in Olkaria the Domes geothermal field

Depth (m)	Depositional sequence (early»late)	Filling type
426	illite»quartz	vein
754	illite»chlorit (unstable)	vesicle
1056	quartz»epidote	vesicle
1118	calcite»quartz	vein
1220	chlorite»quartz»epidote»wollastonite	vesicle
1502	epidote»actinolite	vein
2670	epidote»wollastonite»actinolite	vein

6. FLUID INCLUSION GEOTHERMOMETRY

Fluid inclusions are microscopic vacuoles which are found in minerals and contain geo-fluids. The geo-fluids may be gases, solids, brines or a mixture of any of them. These geo-fluids have microscopic

records of the pressure, composition, and temperature conditions that existed at the time the inclusions were formed. By carefully studying the inclusions in a specially designed fluid inclusion microscope, valuable paleo-thermal information about the geothermal system can be obtained. The paleo-thermal conditions are compared to the alteration mineral temperature and present formation temperature. The alteration mineral temperature plot is obtained by plotting the minimum temperature of the index minerals against the first depth at which these minerals were noted, while the formation temperature is estimated from the recovery temperatures obtained during reservoir temperature logs carried out for some time after the drilling of the well is completed. These temperature plots can also be compared with the boiling point temperature curve of the well. This allows us to evaluate the thermal evolutionary history of the geothermal system.

Primary fluid inclusions are formed during crystallisation of a mineral while secondary inclusions are formed during re-crystallisation of minerals, perhaps in response to micro-fractures. When inclusions are heated in a fluid inclusion microscope, vapour bubbles in the fluid will disappear at the so-called homogenisation temperature, believed to be close to the temperature conditions at the time of entrapment. This will give the paleo-thermal history of the system.

In well OW-914A, a 50 m long depth interval was sampled for mineral grains containing fluid inclusions. This was at 820-870 m depth. Suitable quartz crystals were only found at 836 m depth. Fluid inclusions were analysed in two crystals; a total of 40 secondary fluid inclusions. The homogenisation temperature of the fluid inclusions was between 250 and 290°C, with most of the inclusions homogenising between 250 and 255°C (Figure 14). From this analysis, it is inferred that this was the existing temperature range at the time the quartz fractures healed, after quartz had crystallised. This implies that the system was at this temperature at the time of quartz crystallisation.

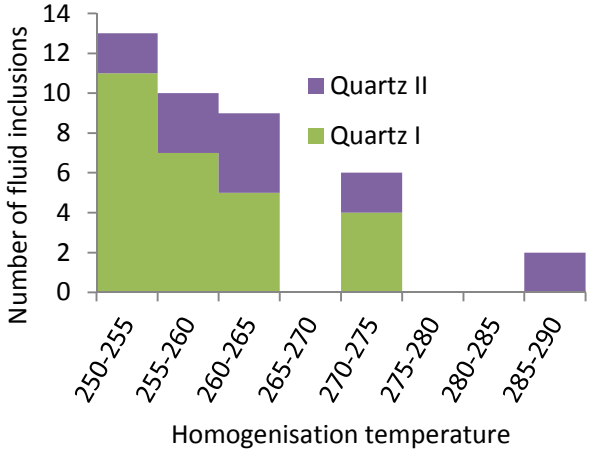

FIGURE 14: Fluid inclusion temperature measurements

Owing to the inadequacy of the available data of the formation temperatures of this well, the evolutionary history was mainly reconstructed using the boiling point curve, alteration minerals, fluid inclusion thermal data and the average discharge rate of this well since it was first discharged two years ago, in August 2010. Alteration index minerals chosen for this comparison were quartz, epidote, prehnite, wollastonite, actinolite and garnet. These minerals, with minimum stability temperatures ranging from 180 to 300°C, were first noted at different depths. These depths and their stability temperatures were used for plotting the alteration temperature curve. After comparing the fluid inclusion homogenisation temperatures, the alteration mineral temperatures, and the boiling point curve (Figure 15), it was inferred that the system has been in a state of equilibrium. The fluid inclusion analyses more or less lie within the alteration mineral temperature curve. This indicates that no significant temperature changes occurred in the time the inclusions were trapped and the alteration minerals formed. Two of the fluid inclusions had homogenization temperatures above the boiling point temperature curve. This number is very small to be solely relied upon to assert that the system was once at boiling conditions, but these two inclusions may be attributed to short lived boiling that might have occurred once in this part of the well. However, further analysis is required to ascertain the boiling conditions. Owing to the limited number of temperature recovery logs, it has been difficult to make a reliable estimate of the formation temperature in well OW-914A; therefore, it is not possible to compare the thermal history in the alteration minerals with the present conditions. However, according to the average rate of discharge of this well, three years after it was discharged in August 2010, it can be inferred that the system is currently under boiling conditions. The average discharge rate ratio of steam against water has been recorded at 2:1, with an average rate of 60 tonnes/hr. of steam against 40

tonnes/hr. of water and a power output of 8 MWe. It is recommended that adequate formation temperature measurements should be carried out in order to ascertain the current thermal state of the system.

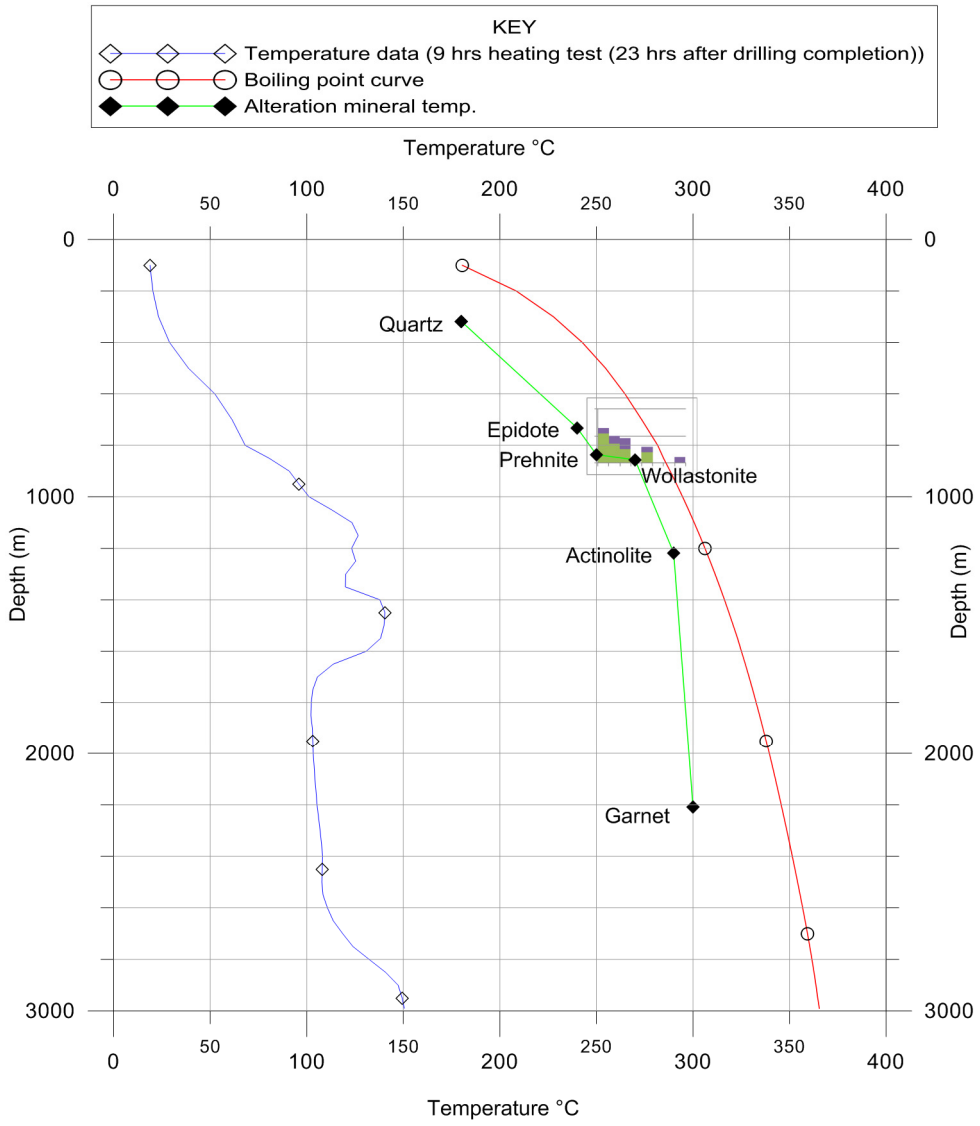

FIGURE 15: Comparison of the fluid inclusion homogenization temperature, boiling point temperature curve and alteration mineral temperature curve

7. AQUIFERS

Permeability in the Olkaria Domes area is mainly enhanced by fractures, joints, lithological contacts and fracture breccias. Aquifers (feed zones) in well OW-914A were located based on the loss of circulation zones, hydrothermal alteration intensity, circulating fluid temperatures and the recovery temperature logs (Figure 16). One of the main aquifers, identified at 2270 m depth (Table 4), was associated with a loss zone which coincides with the fault associated with the inferred collapsed caldera rim of the greater Olkaria volcanic complex. An intermediate aquifer was identified at 2698 m depth, which was associated with a loss zone at the same depth. Some of the aquifers (feed zones) were related to intrusions. A small aquifer noted at 1180 m depth was related to a rhyolitic intrusion at 1154-1162 m depth, an intermediate aquifer at 1390 m depth was related to a basaltic dyke at 1362-1388 m depth, and

another intermediate aquifer noted at 1440 m depth was related to a rhyolitic intrusion at 1438-1440 m depth. An intrusion causes fracturing of the contact rocks, enhancing their permeability. The other aquifers identified were related to lithological contact zones and fracturing of the rocks, as indicated by the presence of micro-veins within the sample cuttings where these aquifers were located. The intermediate aquifers occurring between 1320 and 1620 m depths were associated with fractured rhyolite and trachyte. Some of the circulation losses were encountered at shallow depth (90 m). This is due to the fractured rhyolitic lava that characterises this zone. This zone, with unwanted aquifers, was cased off.

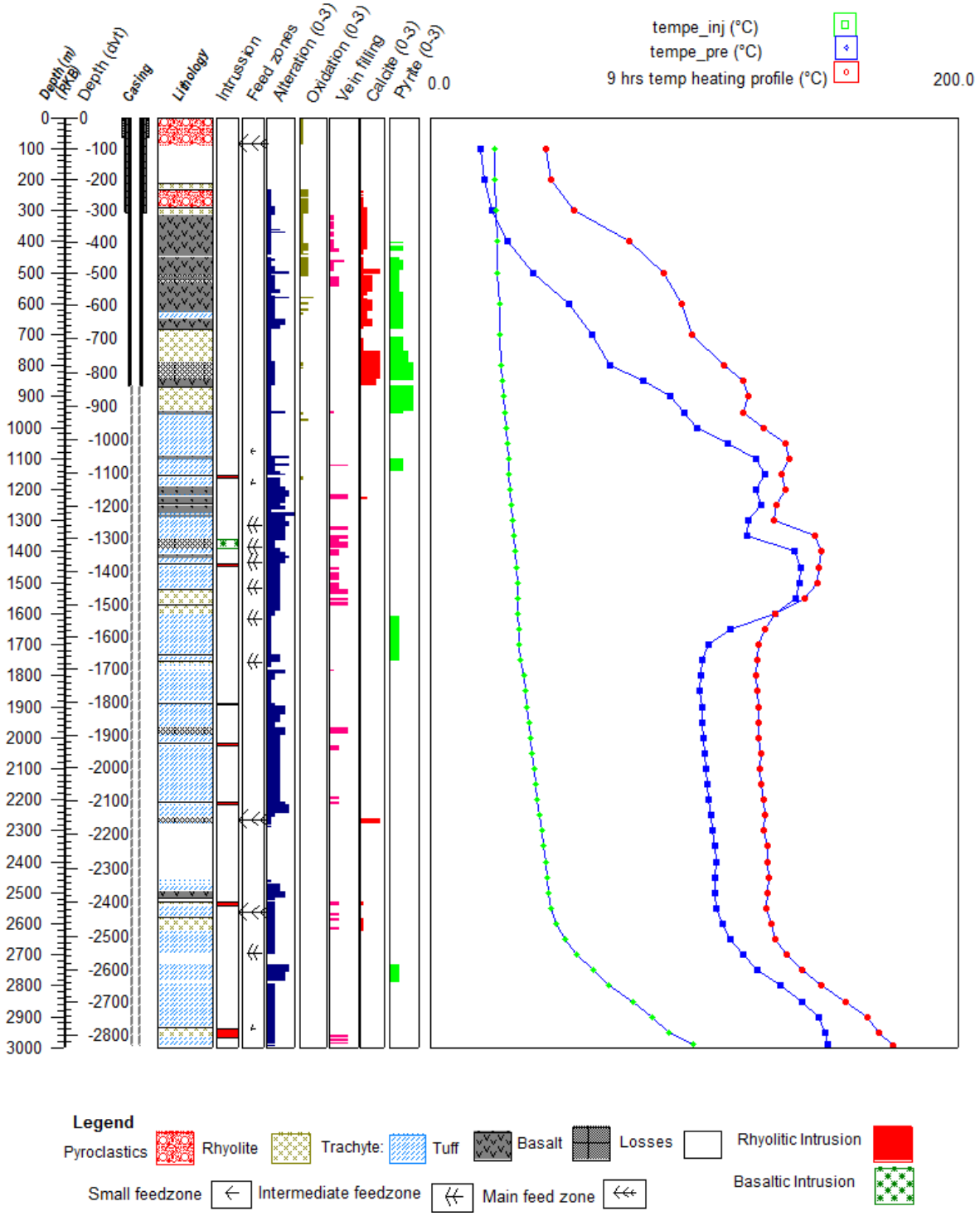

FIGURE 16: Shows the feed zones in OW-914A in relation to the geological properties and the recovery and circulation fluid temperature measurements

TABLE 4: Interpreted aquifers and feed zones based on geological observations and fluid circulation temperature measurements

Depth (m)	Evidence from geological observations and fluid circulation temperatures	Type of aquifer
90-211	Circulation losses, increase in oxidation and alteration intensity, fracture permeability in rhyolites.	Large
1080-1120	Temperature recovery noted, increase in intensity of alteration, abundant calcite. Noted in tuff strata.	Small
1180-1190	Successive temperature recoveries, increased intensity of alteration, fracturing of the tuff and trachyte rocks in this zone.	Small
1320-1340	Increase in intensity of alteration. Noted in the temperature recovery plots.	Intermediate
1390-1400	At the contact between the basaltic intrusion and the trachyte rock. There is increase in intensity of alteration minerals, fracturing of the trachyte. Identified in temperature recovery logs.	Intermediate
1440-1450	At the contact between rhyolitic intrusion and a trachyte rock. Highly fractured trachyte rock. Identified in temperature recovery logs.	Intermediate
1520-1620	This is an aquifer characterized with two feed zones at 1520 and 1620 m depth. The feed zones are at the contact between rhyolite and trachyte rock. The aquifer is characterized by fractured rhyolitic rock. Relatively high alteration intensity and abundant calcite noted.	Intermediate
1780-1800	Loss of circulation, increase in alteration intensity.	Intermediate
2270-2460	Loss of circulation, increase in alteration intensity, abundant calcite. Identified in temperature recovery logs.	Intermediate
2570-2590	Fracturing of the trachyte rock. Identified in temperature recovery logs.	Large
2698-2734	Loss of circulation, increase in alteration intensity. Identified in temperature recovery logs.	Large
2940-2950	Fractured trachytic rock observed, occurs at contact between trachyte and rhyolite intrusion. Noted in temperature recovery logs.	Large

Figure 16 shows the aquifers identified in this well, based on the circulation fluid temperature data, recovery temperature logs, loss zones and alteration. The first curve is the temperature pre-injection log, done for 13 hours, immediately after drilling was completed. It appears more or less linear but with observable temperature changes. The two curves are temperature injection logs done for 9 hours each, 13 and 22 hours after drilling was completed, respectively. They show conspicuous changes in temperature at different depths of the well. These temperature changes indicate feed zones and/or aquifers. Thirteen aquifers (large, intermediate and minor) were identified in this well. Three main (4 large aquifers noted in Table 4) aquifers were identified, seven intermediate aquifers and three small aquifers (also called feed zones). These zones were characterised by an increase in the intensity of alteration, a change in circulating fluid temperature, change in recovery temperature logs and or circulation loss. Most of these zones were also characterised by fracturing. This was evident by micro-veins identified in the sample cuttings that coincided with these feed zones. Table 4 gives a summary of the aquifers identified in well OW-914A.

8. DISCUSSION

The surface geology of Olkaria geothermal field is mainly characterised by acidic comenditic lavas and pyroclastics while the subsurface geology is mainly characterised by trachytes, basalts, rhyolites and tuffs. The lithology of well OW-914A, based on the analysis of drill cuttings, comprises five main rock formations: pyroclastics, tuff, basalt, rhyolite and trachyte. These formations are classified according to their texture and mineralogy. A magma chamber exists under the Olkaria volcanic complex between 7-10 km as observed from both geological and geophysical studies (Omenda, 2000). The occurrence of tuff, rhyolite and basalt at a near-surface depth and trachyte at a deeper level in this well relate well with an earlier explanation by Omenda (2000). He related the occurrence of acidic (comenditic) lava on the

surface and near-surface, and trachyte at deeper levels, to the high differentiation that happened in this magma chamber. The stratigraphy in well OW-914A also relates well with the stratigraphic column of the greater Olkaria volcanic complex as explained by Shackleton (1986), Omenda (2000) and Ogoso-Odongo (1986). They proposed the surface and near-surface geology to be dominated by pyroclastics and comenditic lavas, of the upper Olkaria volcanics. In this well, the shallow depth is dominated by pyroclastics and rhyolite lavas down to a depth of 500 m. This was also noted in wells OW-916 and OW-912B. However, well OW-911A had trachyte at shallow depth from about 180 m down to 270 m depth, and again from about 450 m down to 500 m depth. The trachyte strata in OW-911A is intercalating with rhyolite and tuff. From about 100 m down to 250 m, losses were experienced in all four wells, an indication that the near-surface rocks are highly fractured in this area. Layers of tuff are also observed intercalating with the rhyolite at the near-surface. These are thicker layers than the tuff layers that occurred below 1200 m. Wells OW-914A and OW-916 had the thickest layers with 200 m and 175 m, respectively, occurring between 200 m down to 1200 m depth. Well OW-912B had about a 125 m thick layer of tuff at this depth while well OW-911A had less than a 50 m thick layer of tuff at 1200 m depth from the surface. Some of the pyroclasts and tuff are said to have come from the Longonot and Suswa volcanic eruptions. Basalt was first encountered at 506 m in well OW-914A. It relates to the Olkaria basalt, which is proposed to be the cap rock for the Olkaria geothermal system. This layer of basalt at around 500 m depth is thin in the Domes area. It occurs with a thickness of less than 50 m as observed in wells OW-901, OW-902, OW-903, OW-911A, OW-912B, OW-916 and OW-914A. This basalt layer can be used as a marker horizon, when carrying out analyses of drill cuttings, to infer buried faults in this area. Trachyte was the dominant rock at greater depth, an observation noted in all four wells, with a 26 m thick stratum being observed at 624 m depth but thicker strata from 950 m down to the bottom of well OW-914A. This relates to the plateau trachytes which have been noted to occur in the geothermal complex at a depth between 1000 and 2600 m. The intermittent occurrence of tuff layers, intercalating with other lithological units, may indicate that in the past this area experienced multiple episodes of eruptions. Each eruption began by the eruption of ash material, forming layers of tuff, followed by a magma eruption overlaying the tuff layer. Eight intrusions were recognised, with one of them being a basaltic dyke and the other seven rhyolitic intrusions. The basaltic and rhyolitic intrusions were all fine-grained with characteristic chilled margins showing high alteration and/or oxidation at the contact zones of the rocks below and above. The intrusions had similar characteristics, an indication that they may be from a similar intrusive phase which resulted in numerous intrusions cutting across the lithology in this area. This intrusive phase may be the same phase that formed the dome-like structures of rhyolitic composition, which are aligned along the loci of the hypothesised collapsed caldera rim. Further analyses on the composition of these intrusions and the dome-like structures are needed to ascertain this.

There is a systematic occurrence of hydrothermal alteration minerals with depth. Low-temperature minerals were noted at shallow depths, with subsequent higher temperature alteration minerals occurring with increasing depth. This indicates increasing alteration temperature with depth. For instance, quartz was found near the surface at 318 m depth, while actinolite and garnet, both high-temperature minerals, first appeared at 1218 and 2208 m depth, respectively. Five alteration mineral zones were identified in well OW-914A: an un-altered zone 0-90 m depth; the zeolite-illite zone 90-480 m depth; a chlorite-illite zone 480-732 m depth; an epidote-chlorite-illite zone 732-1218 m depth and an actinolite-epidote-chlorite-illite zone 1218-2996 m depth. The occurrence of high-temperature alteration minerals like epidote, actinolite and wollastonite indicates that the formation temperature is well over 240°C. A comparison was made between the depths at which alteration minerals occurred in wells OW-911A, OW-916, OW-912B and OW-914A. There were similarities in the trend of occurrence of the alteration minerals with depth in the four wells, with minerals formed at relatively lower temperatures at near-surface, and relatively higher temperature ones at depth, albeit at different depths in the four wells (Figure 17). However, well OW-912B had garnet appearing at a shallower depth of about 1100 m compared to wollastonite and actinolite which occurred below this depth. This may be attributed to boiling at this depth. The boiling was as a result of a rhyolitic intrusion, which elevated temperatures locally, resulting in the deposition of garnet, which starts to form at a higher temperature than actinolite and wollastonite. A thermal cross-section drawn across these wells along line A-B indicates that the

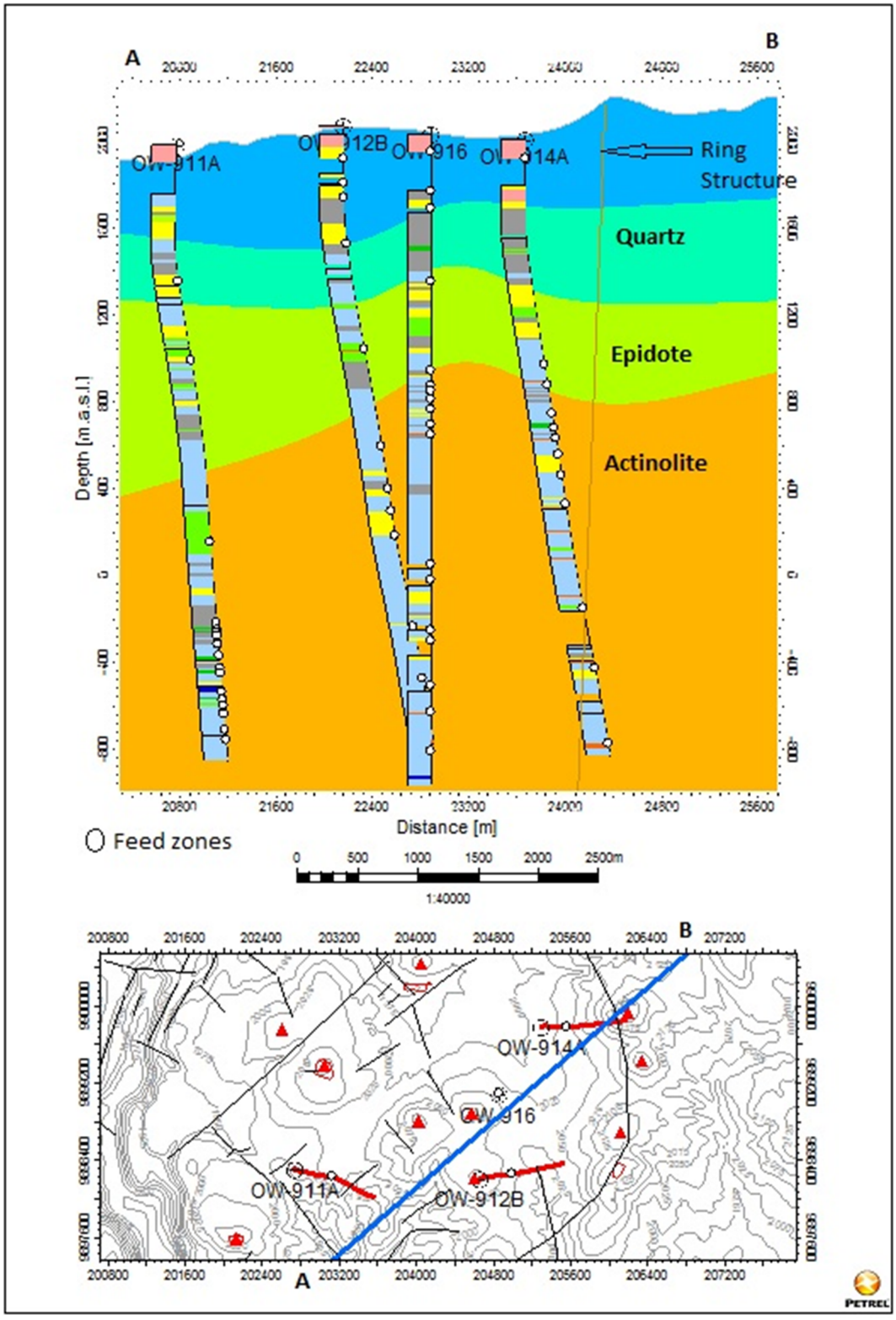

FIGURE 17: A thermal cross-section between line A-B cutting across wells OW-914A, OW-916, OW-912B and OW-911A, generated basing on the depth at which the selected index minerals were first noted, the ring structure and aquifer distribution (the area to the northeast of OW-914A along line AB is extrapolated)

area around wells OW-914A and OW-916 has higher temperatures near the surface whereas the area trending towards wells OW-912B and OW-911A has higher temperatures only occurring at greater depth (Figure 17). This indicates that well OW-911A lies on the boundary of the Domes geothermal field.

Fluid inclusion studies indicate that the geothermal system in the Domes area has remained in a state of thermal equilibrium over time. The 40 fluid inclusions at 836 m depth were analysed and had homogenisation temperatures of between 250 and 290°C, which falls within the temperature of the alteration minerals found at the same depth as the quartz crystals selected for the fluid inclusion analysis. Two of the fluid inclusions had homogenisation temperatures above the boiling point temperature curve at 836 m depth. However, this number was too small to be solely relied upon in asserting that the system was once at boiling conditions. These two inclusions may be attributed to short lived boiling that might have occurred once in this part of the well. An alteration mineral sequence indicated a pro-grade deposition from lower to higher temperature alteration minerals. Fine-grained clays appeared, succeeded by coarse-grained clays, and then epidote. From these analyses, it is inferred that the system has been in a state of equilibrium. The fluid inclusion analyses more or less lie within the alteration mineral temperature curve. This indicates that no significant temperature changes have occurred from the time the inclusions were trapped to the time alteration minerals started forming. Owing to the limited number of temperature recovery logs, it has been difficult to make a reliable estimate of the formation temperatures in well OW-914A; therefore, it is not possible to compare the thermal history in the alteration minerals to the present conditions. However, from the average rate of discharge of the well in the 2 years since it was discharged, it can be inferred that the well is under boiling conditions. The average mass rate of 60 tonnes/hr. of steam against 40 tonnes/hr. of water was recorded in the two years from August 2010 to the present, September 2012. The well has a power output of 8 MWe.

The aquifers in well OW-914A are mainly associated with fractures, lithological boundaries, loss zones and highly fractured rocks. These zones are associated with high permeability. One of the main aquifers in well OW-914A, at 2270 m depth, was found to coincide with the location of the fault interpreted to belong to the ring structure (Figure 17). This is believed to be the caldera rim along which eruptions of domes of rhyolitic composition formed a ring-like dome structure. Some of the smaller feed zones were mainly located at lithological boundaries (contact zones), while others were associated with the intrusions. An intrusion causes fracturing of the adjacent rocks, increasing their permeability. A comparison of the location of aquifers between wells OW-911A, OW-912B, OW-916 and OW-914A exposes the role of permeability and porosity in the formation of aquifers. Most of the aquifers located in this well are associated with the tuff, rhyolite and loss zones, while some of the main aquifers also exhibit a relationship with fractures. From drill cutting analyses of these wells, it was observed that the tuff associated with aquifers is highly vesicular at shallow depths (250-600 m). The rhyolite associated with aquifers is highly fractured and mainly occurs between 250-2200 m where many of these aquifers are located. The fracturing of the rhyolite and the vesicular nature of the tuffs enhances permeability, hence, the association of most of these aquifers with these strata.

9. CONCLUSIONS

From the analysis of the samples and data for well OW-914A, the following conclusions can be drawn:

- The lithology of well OW-914A mainly comprises five rock types: pyroclastics, tuff, rhyolite, trachyte and basalt. Basalt occurs in small units with trachyte being the dominant rock at greater depth.
- A basaltic intrusion occurs at 1364-1388 m depth. It is fine-grained with chilled margins.
- Rhyolitic intrusions occur at 1154 m and show intermittent occurrence down to the bottom of the well at 2938 m depth. They are fine-grained with chilled margins and show high oxidation at the contact with the country rock. These rhyolitic intrusions may indicate that there may have existed

an intrusion phase, which resulted in numerous intrusions which cut across the lithological units in this area. This intrusive phase may be the same phase which resulted in the formation of the dome-like ring structure of rhyolitic composition, along the loci of the hypothesised collapsed caldera rim.

- Three parameters control alteration in this field: primary rock type, temperature and permeability. Five alteration mineral zones were identified in this well: an un-altered zone (0-90 m); a zeolite-illite zone (90-480 m); a chlorite-illite zone (480-732 m); an epidote-chlorite-illite zone (732-1218 m) and an actinolite-epidote-chlorite-illite zone (1218-2996 m). The temperature in the Domes area increases with depth as shown by the occurrence of higher temperature minerals with increasing depth in this well, as well as in the other three wells in this area.
- Sequences of mineral deposition, coupled with fluid inclusion analysis and boiling temperature curve, indicate that the system has been at equilibrium. There has been no significant temperature change in the system; the fluid inclusions analysis more or less falls within the alteration mineral temperature plot. Due to a limited number of temperature or temperature recovery logs, it has been difficult to make a reliable estimate of the formation temperature in well OW-914A; therefore, it is not possible to compare the thermal history in the alteration minerals with present conditions. However, from the average rate of discharge of 68 tonnes/hr. of steam against 32 tonnes/hr. of water from the well over the 2 years since it was discharged, it can be inferred that the well is under boiling conditions.
- Aquifers and feed zones are associated with fractures, fractured rocks, vesicular rocks, loss zones, intrusions and lithological contacts. The intermediate and main aquifers are associated with loss zones, fractures, fractured rhyolite and intrusions. The first main aquifer at 90 m was located within a highly fractured rhyolite; the second one was located at a fracture of the ring structure at 2270 m; the last one occurred within a rhyolitic intrusion observed at 2530 m. The intermediate aquifers located between 1320 and 1760 m were mainly located within vesicular tuff and fractured rhyolite; one feed zone at 1340 m occurred next to a basaltic dyke. The small aquifers were associated with vesicular tuff at shallow depth of 1080 m, and rhyolite intrusions encountered at 1180 and 2940 m depth.

ACKNOWLEDGEMENTS

I take this opportunity to express my sincere gratitude to the United Nations University and the government of Iceland for having granted me this golden opportunity to hone my skills in geothermal energy exploitation. Special thanks go to the director of the UNU-GTP, Dr. Ingvar B. Fridleifsson, deputy director, Mr. Lúdvík S. Georgsson, Ms. Thórhildur Ísberg, Mr. Ingimar G. Haraldsson, Mr. Markús A.G. Wilde and Málfrídur Ómarsdóttir for their coordinated assistance to see me through this course with minimal hitches. I extend my gratefulness to my supervisors, Ms. Anette K. Mortensen, Dr. Björn S. Hardarson and all the other ISOR staff with special thanks to Dr. Hjalti Franzson, Mr. Steinþór Níelsson and Dr. Gudmundur H. Gudfinnsson for their guidance, critical comments and valuable input during data analysis for this project. I also thank Dr. Gudmundur Ómar Fridleifsson for his lesson and guidance on geological exploration for geothermal features at the Geitafell Volcanic complex. Your vast knowledge in geological exploration for geothermal resources was of great value in adding to my geothermal skills.

I am indebted to Kenya Electricity Generating Company (KenGen) management office for granting me leave to attend this course and for allowing me to use the company data for my project. Thanks to my colleagues in the company for helping me in mobilising the required data whenever I called upon them back home.

To the 2012 UNU fellows, you are great people. You made me feel at home away from home and I am grateful to you all. We all had our input but God made it possible for us all.

REFERENCES

Ambusso, W.J., and Ouma, P.A., 1991: Thermodynamic and permeability structure of Olkaria Northeast field: Olkaria fault. *Geothermal Resource Council Transactions*, 15, 237-242.

Baker, B.H., 1987: Outline of the petrology of the Kenya rift alkaline province. In: Fitton, J.G., and Upton, B.G.J. (eds.), *Alkaline igneous rocks*. *Geol. Soc., Spec. Publ., 30*, 293-311.

Baker, B.H., Mitchel, J.G., and Williams, L.A.J., 1988: Stratigraphy, geochronology and volcano-tectonic evolution of the Kedong-Naivasha-Kinangop region, Gregory Rift Valley, Kenya. *Geological Society of London, 145,* 107-116.

Baker, B.H, Mohr, P.A, and Williams, L.A.J., 1972: Geology of the Eastern Rift System of Africa. *Geological Society of America, Special Paper 136,*1-67.

Baker, B.H., and Wohlenberg, J., 1971: Structural evolution of the Kenya Rift Valley. *Nature, 229,*538-542.

Bechtel, T.D., Forsyth, D.W., and Swain, S.W., 1987: Mechanism of isostatic compensation in the vicinity of the East Africa Rift, Kenya. Geophysics, 90, 445-465.

Browne, P.R.L., 1978: Hydrothermal alteration in active geothermal fields. *Annual Review Earth and Planetary Sciences,6,* 229–250.

Browne, P.R.L., 1984: Subsurface stratigraphy and hydrothermal alteration of the eastern section of the Olkaria geothermal field, Kenya. *Proceedings of the 6th New Zealand Geothermal Workshop, Geothermal Institute, Auckland,* 33-41.

Clarke, M.C.G., Woodhall, D.G., Allen, D., and Darling G., 1990: *Geological, volcanological and hydrogeological controls on the occurrence of geothermal activity in the area surrounding Lake Naivasha, Kenya, with coloured 1:100 000 geological maps.* Ministry of Energy, Nairobi, 138 pp.

Franzson, H., 2012: *Borehole geology.* UNU-GTP, Iceland, unpublished lecture notes.

Gebrehiwot M., K.., 2010. *Subsurface geology, hydrothermal alteration and geothermal model of northern Skardsmýrarfjall, Hellisheidi geothermal field.* University of Iceland, MSc thesis, UNU-GTP, report 5, 65 pp.

Haukwa, C.B., 1984: *Recent measurements within Olkaria East and West fields*. Kenya PowerCo., internal report, 13 pp.

Henry, W.J., Mechie, J., Maguire, P.K.H., Khan, M.A., Prodehl, C., Keller, G.R., and Patel, J., 1990: A seismic investigation of the Kenya rift valley. *Geophysics J. Int., 100-1,* 107-130.

KenGen, 2000: *Conceptual model of Olkaria geothermal field*. KenGen, Kenya, compiled by Muchemi, G.G., internal report, 13 pp.

KenGen 2012: *Geological well logging report for well OW-915B*. KenGen, Kenya, internal report.

Lagat, J.K., 2004: *Geology, hydrothermal alteration and fluid inclusion studies of the Olkaria Domes geothermal field, Kenya.* University of Iceland, MSc thesis, UNU-GTP, Iceland, report 2, 71 pp.

Macdonald, R., 1974: Nomenclature and petrochemistry of the peralkaline oversaturated extrusive rocks. *Bull. Volcanology, 38*, 498-516.

MacDonald, R., Black, H.E., Fitton, J.G., Marshall, A.S., Nejbert, K., Rodgers, N.W., and Tindle, A.G., 2008: The roles of fractional crystallization, magma mixing, crystal mush remobilization and volatile-melt interactions in the genesis of a young basalt-peralkaline rhyolite suite, the Greater Olkaria volcanic complex, Kenya Rift Valley. *J. Volcanology, 49-8,* 1515-1547.

MacDonald, R., Black, S., Fitton, J.G., Rogers, N.W., and Smith, M., 2001: Plume-lithospheric interactions in the generation of the basalts of the Kenya Rift, East Africa. *J. Petrology, 42,* 877-900.

MacDonald, R., Davies, G.R., Bliss, C.M., Leat, P.T., Bailey, D.K., and Smith, R.L., 1987: Geochemistry of high silica peralkaline rhyolites, Naivasha, Kenya rift valley. *J. Petrology, 28,* 979-1008.

Mariita, N.O., 2009: Exploration history of Olkaria geothermal field by use of geophysics. *Paper presented at "Short Course IV on Exploration for Geothermal Resources", organized by UNU-GTP, KenGen and GDC, Lake Naivasha, Kenya,* 13 pp.

Marshall, A.S., MacDonald, R., Rogers, N.W., Fitton, J.G., Tindle, A.G., Nejbert, K., and Hinton, R.W., 2009: Fractionation of peralkaline silicic magmas: the Greater Olkaria volcanic complex, Kenya Rift Valley. *J. Petrology, 50*,323-359.

Middlemost, E.A.K., 1989: Iron oxidation ratios, norms and classification of volcanic rocks. *Chemical Geology, 77,* 19-26.

Muchemi, G.G., 1999: *Conceptual model of the Olkaria geothermal field*. KenGen, internal report, 19 pp.

Mungania, J., 1992: *Preliminary field report on geology of Olkaria volcanic complex with emphasis on Domes area field investigations*. Kenya Power Co., internal report.

Mungania, J., 1999: *Summary of the updates of the geology of Olkaria Domes geothermal field*. KenGen, Kenya, internal report.

Mwangi, M.N., 1984: *A review of geophysical data of Olkaria geothermal field for STRM Nov. 1984.* Kenya Power Co., report KPC/4P/OW/007.

Naylor, W.I., 1972: *Geology of the Eburru and Olkaria prospects*. UN Geothermal Exploration Project, report.

Ogoso-Odongo, M.E., 1986: Geology of Olkaria geothermal field. *Geothermics*, *15*, 741-748.

Omenda, P.A., 1994: The geological structure of the Olkaria west geothermal field, Kenya. *Proceedings of the 19th Stanford Geothermal Reservoir Engineering Workshop, Stanford University, Stanford, Ca,* 125-130.

Omenda, P.A., 1998: *The geology of well OW-901*. KenGen, internal report.

Omenda, P.A., 2000: Anatectic origin of comendite in Olkaria geothermal field, Kenya Rift; Geothermal evidence of syenitic protholith. *African J. Science & Technology, Science & Engineering Series, 1,* 39-47.

Onacha, S.A., 1993: *Resistivity studies of the Olkaria-Domes geothermal project*. KenGen, internal report.

Shackleton, R.M., 1986: Precambrian collision tectonics in Africa. In: Coward, M.P., and Ries, A.C. (eds.), *Collision tectonics. Geol. Soc. Spec. Publ., 19,* 329-349.

Simiyu, S.M., and Keller, G.R., 1997: An integrated analysis of lithospheric structure across the East African plateau based on gravity anomalies and recent seismic studies. In: Fuchs, K., Altherr, R., Müller, B., and Prodehl, C. (eds.), *Structure and dynamic processes in the lithosphere of the Afro-Arabian rift system*. *Tectonophysics*, 278, 291-313.

Simiyu, S.M., Oduong, E.O., and Mboya, T.K., 1998: *Shear wave attenuation beneath the Olkaria volcanic field.* KenGen, internal report.

Simiyu, S.M., Omenda, P.A., Keller, G.R and Antony, E.Y., 1995: Geophysical and geological evidence of the occurrence of shallow intrusion in the Naivasha sub-basin of the Kenya rift. *AGU Fall 1995 meeting, Abst*., F657, V21A-12.

Smith, M., and Mosley, P., 1993: Crustal heterogeneity and basement influence on the development of the Kenya rift, East Africa. *Tectonics, 12,* 591-606.

Stuart, F.S., and Browne, P.R.L., 2000: Hydrothermal minerals and precious metals in the Broad lands-Ohaaki geothermal system: Implication for understanding low-sulfidation epithermal environments. *Economic Geology J., 95-5*, 971-999.

Williams, L.A.J., 1972: The Kenya rift volcanics: a note on volumes and chemical composition. *Tectonophysics, 15*, 83-96.

APPENDIX I: Details of the lithological units encountered in OW-914A

Depth	Rock description	Rock type	Secondary minerals
0-90	Brownish to yellow fresh highly pumiceous material mixed with volcanic glass. Non-crystalline volcanic glass. Sanidine phenocrysts noted in the glassy matrix. Highly oxidized, palagonite noted.	Pyroclastics	Oxides
90-211	Loss of returns	-	-
211-226	Whitish fine- to medium-grained slightly porphyritic lava. Has quartz phenocrysts embedded in the ground mass highly dominated by finely-grained quartz. Slightly oxidized to reddish brown oxides. Has pyroxenes radiating from a central point together with quartz in a spherulitic manner. Vesicles filled with silica and scolecite.	Rhyolite	Oxides Opal Chalcedony Scolecite
226-290	Fine-grained brown yellow, pumiceous and highly vesicular slightly porphyritic lava. Highly heterogeneous with mixture of different mineral grains (rhyolite, volcanic glass, tuff fragments and pumice). Pyroxene phenocrysts noted. Slightly altered to fine-grained brown and green clays. Some of the fragments show rounding, an effect of transportation from a distance before deposition. Calcite noted in small amounts.	Pyroclastics	Calcite Clays Oxides Mesolite/ Scolecite
292-312	Fine-grained reddish brown to white lava. Phenocrysts of quartz and sanidine and pyroxenes noted in the groundmass. The phenocrysts show a spherulitic texture, radiating from a central point outwards. It is moderately oxidized to brown oxides. Slightly altered to green and brown clays. Scolecite noted filling in vesicles (course-grained, tabular thin elongated prisms with reddish brown oxides covering the grains).	Rhyolite	Oxides Clays Calcite Scolecite
312-408	Fine non-crystalline, grained glassy green tuff. It is highly vesicular with some of the vesicles being filled with calcite. It has a mix of volcanic glass and few crystals of rhyolite mineral grains. Silica noted in the vesicles. Slight to moderate oxidization. Mafic minerals also embedded in the highly glassy ground, mass material.	Glassy tuff	Pyrite Clays Oxides Chalcedony

Depth	Rock description	Rock type	Secondary minerals
418-428	Greenish fine-grained lava with sanidine fragments embedded in the lithic material. It is highly vesicular. Abundant pyrite with well-formed cubes. Calcite deposited in the vesicles. It is slightly oxidized to brown clays. Quartz grains noted in the ground mass.	Lithic tuff	Clays Quartz Calcite Clays, Pyrite
428-442	Greenish white fine-grained lava. It is layered and highly vesicular. Has micro-veins filled with green clays. Calcite is noted deposited in the vesicles. Well-developed pyrite grains are embedded in the lithic ground mass.	Welded tuff	Clays, Quartz Calcite Clays Pyrite
442-454	White fine-grained lava. It has fragments of quartz embedded in the ground mass. It is slightly altered to white, green and brown clays. Pyrite is disseminated in the groundmass.	Lithic tuff	Oxides, Quartz Pyrite, Clays Calcite
454-458	Green fine-grained lava. It appears in layers. It is moderately oxidized and has mafic minerals disseminated in the lithic material. Pyrite is disseminated in the ground mass. It is slightly altered to brown clays.	Welded tuff	Oxides Calcite Clays Pyrite
458-460	White fine-grained lava. Has grey matrix with quartz fragments embedded in the groundmass. It is slightly altered to coarse-grained brown and white clays.	Lithic tuff	Oxides Calcite Clays, Pyrite
460-464	Brown to greenish fine-grained lava. It appears layered. Mafic minerals form the lithic fragments. The lithic fragments show elongation. It is slightly oxidized. It is slightly altered to brown and green coarse-grained clays.	Welded tuff	Clays Oxides Calcite Pyrite
464-466	Green to white fine-grained lave. It has abundant quartz grains filling the vesicles. It shows moderate alteration to brown and white clays. It is moderately oxidized to brown oxides. It shows layering.	Welded tuff	Clays Quartz calcite Oxides, Pyrite
466-490	Green to grey fine-grained lava. It shows moderate alteration to brown and green fine and coarse-grained clays. It has abundant pyrite embedded in the groundmass.	Lithic tuff	Clays Quartz calcite Oxides, Pyrite
490-510	Brownish fine-grained highly altered lava. Pyrite crystals embedded in the ground mass. Moderately altered to greenish brown clays.	Lithic tuff	Clays Quartz calcite Oxides, Pyrite
510-514	Dark greenish grey fined to medium-grained lava. It is moderately oxidized to brown oxides. It has fine-grained brown/green clay deposited in the vesicles.	Basalt	Pyrite, Calcite Quartz Clays
514-544	Grey to green fine-grained lava. It has lithic fragments with sanidine embedded in the ground matrix. Calcite noted in the vesicles. It shows moderate oxidation to brown clays.	Lithic tuff	Pyrite Calcite Quartz, Clays
524-534	Dark grey to green fine- to medium-grained lava. The vesicles are filled with calcite and moderately altered to fine-grained brown clays.	Basalt	Calcite, Quartz Clays, Oxides
534-554	Grey to brown highly vesicular fine-grained lava. It has lithic fragments of quartz and mafic minerals embedded in the groundmass. It shows high alteration to green and white fine-grained clays. It has quartz and calcite filling in the vesicles.	Lithic tuff	Clays Quartz calcite Oxides Pyrite
554-564	Brown to green fine-grained lava. It is rich in lithic ash material which forms the groundmass. Lithic fragments of quarts mineral grains are embedded in the groundmass. It is moderately altered to fine-grained brown and green clays. It is highly vesicular with fine to coarse-grained clays filling in the vesicles. It is slightly oxidized.	Lithic tuff	Clays Quartz calcite Oxides Pyrite
564-586	White to brown fine-grained highly vesicular lave. It has pyroxene mineral grains embedded in the ash ground mass. It shows moderate to high alteration to brown and white fine-grained clays.	Lithic tuff	Clays Quartz calcite Oxides Pyrite
586-624	Brown to grey white fine-grained lava. It is heterogeneous with a mix of trachyte, basalt and tuff grains present. The tuff crystals are the	Lithic tuff	Clays Quartz calcite Oxides

Depth	Rock description	Rock type	Secondary minerals
	dominant grains; they are grey in colour with sanidine, quartz and pyroxene embedded in the ground mass.		Pyrite
624-650	Fine- to medium-grained brownish lava. It is highly porphyritic. Has sanidine grains forming the bulk of the phenocrysts. Mafic minerals form a small percentage of the phenocrysts. It shows moderate alteration to green fine-grained clays. Calcite is in moderate abundance.	Trachyte	Calcite Clays
650-682	White to brown fine-grained lava. It has ash as the lithic material with mafic minerals and sanidine feldspars forming the lithic fragments. It is highly vesicular. The vesicles are filled with well-developed quartz crystals. It is slightly altered to fine-grained white and brown clays and green coarse-grained clays.	Lithic Tuff	Calcite Quartz Calcite Pyrite, Calcite
682-792	Fine- to medium-grained brownish lava. The phenocrysts are in less abundance and are mainly quartz. The groundmass is mainly composed of finely-grained quartz and minute quantities of pyroxenes and sanidine. Epidote is noted at 732 m. It is slightly altered to fine-grained green and brown clays. Wairakite is noted 762 m.	Rhyolite	Quartz Clays Calcite Epidote Wairakite
792-846	Medium-grained highly porphyritic green to dark grey lava. Phenocrysts are mainly quartz and mafic minerals. Has abundant calcite with pyrite disseminated in the groundmass. The vesicles are filled with epidote and wairakite. It shows slight alteration to fine-grained green clays.	Basalt	Clays Quartz Calcite Epidote Wairakite Prehnite
846-866	Light green to white fine-grained lithic lava. It has the vesicles filled with epidote, wairakite and quartz. It shows slight to moderate alteration to fine-grained green clays. It has abundant calcite	Tuff	Clays, Calcite Quartz Wairakite Epidote Prehnite Wollastonite
866-946	White coloured fine-grained slightly porphyritic lava. It has quartz phenocrysts in the groundmass. It shows slight intensity of alteration to green clays.	Rhyolite	Wairakite Quartz, Clays
946-956	Brown to grey fine-grained lithic lava. It has lithic fragments of quartz and mafic minerals embedded in the groundmass. The vesicles are filled with quartz, epidote and clays.	Lithic tuff	Clays, Quartz wairakite Epidote Prehnite
956-1154	Grey to brown fine- to medium-grained lava. It is quite massive and highly porphyritic. It has sanidine phenocrysts embedded in the ground mass. Pyroxene mineral grains also occur as phenocrysts within the ground mass. Tuff mineral grains are also found in this sample. It shows moderate to high intensity of alteration to brown fine-grained clays.	Trachyte	Clays, Quartz Wairakite Epidote Prehnite Wollastonite
1154-1162	White fine-grained lava. It is slightly porphyritic with quartz crystals occurring as phenocrysts embedded in the groundmass. The groundmass has chilled fine grains. It is relatively fresh. Brown fine-grained clays noted.	Rhyolitic intrusion	Clays
1162-1190	Grey to brown medium-grained lava. It is highly porphyritic with pyroxenes and sanidine phenocrysts embedded in the ground mass. It shows high intensity of alteration to brown clays.	Trachyte	Clays, Quartz Epidote Wollastonite
1190-1200	Brown fine-grained well compacted lithic lava. It has highly altered lithic fragments in the groundmass. It is quite massive and highly altered to brown fine-grained clays.	Lithic tuff	Clays Quartz
1200-1208	Grey fine- to medium-grained highly porphyritic lava. It has sanidine phenocrysts embedded in the ground mass. Amphiboles noted occurring as phenocrysts.	Trachyte	Clays, Epidote Quartz Wollastonite

Depth	Rock description	Rock type	Secondary minerals
1208-1216	Brown fine-grained tuffaceous lava. Feldspar forms lithic fragments. Highly altered to brown clays.	Lithic tuff	Clays, Quartz Titanite
1216-1226	Grey to white fine- to medium-grained lava. It has sanidine phenocrysts in the groundmass. The sanidine phenocrysts show orientation in flow-like texture.	Trachyte	Clays, Quartz Epidote Actinolite
1226-1244	Grey to green fine-grained lava. It is heterogeneous lava with trachyte and tuff mineral grains. Tuff grains are in abundance. The grains are scoria-like. Sanidine phenocrysts are present. Moderately altered to green fine-grained clays.	Lithic tuff	Clays Quartz Epidote Actinolite
1244-1252	Whitish grey medium-grained highly porphyritic lava. Lithic fragments of mafic minerals and sanidine present. They show flow texture. Highly altered to brown clays.	Trachyte	Clays, Quartz Epidote Wollastonite
1252-1262	Fine-grained tuffaceous lava with lithic fragments of quartz and feldspars forming lithic fragments. It is mixed lava with trachyte mineral grains observed. Highly altered to brown clays.	Lithic tuff	Clays Quartz Epidote
1262-1272	Fine- to medium-grained brown grey to grey highly porphyritic lava. Has sanidine and mafic mineral phenocrysts orientated in a preferred direction.	Trachyte	Clays Actinolite
1272-1276	Grown fine-grained tuffaceous lava. Quartz lithic fragments observed.	Lithic tuff	Clays, Quartz Epidote Actinolite
1276-1282	Fine- to medium-grained brown grey to grey highly porphyritic lava. Has sanidine and mafic mineral phenocrysts showing orientation in a direction.	Trachyte	Clays Actinolite
1282-1286	Grown fine-grained tuffaceous lava. Quartz lithic fragments observed.	Lithic tuff	Clays, Quartz Epidote Actinolite
1286-1362	Brownish white fine- to medium-grained highly porphyritic lava. Phenocrysts of pyroxene, sanidine, and quartz noted. Flow texture observed. Slight to moderate alteration to brown and green fine-grained clays.	Trachyte	Clays, Quartz Wollastonite Actinolite
1362-1388	Dark grey-green medium-grained lava. Abundant mafic phenocrysts. It is mixed lava with trachyte grains noted in the sample. It is relatively fresh with chilled margins.	Basaltic intrusion	Clays, Quartz Epidote Actinolite
1388-1414	Light grey medium-grained highly porphyritic lava. Phenocrysts of sanidine and mafic minerals. Highly altered to brown clays.	Trachyte	Clays, Quartz Epidote Actinolite
1414-1420	Brown fine-grained tuffaceous material. Mafic minerals and feldspars form lithic fragments. Slightly vesicular.	Lithic tuff	Clays, Quartz Epidote Actinolite
1420-1438	Medium-grained highly porphyritic lava. Mafic minerals and sanidine phenocrysts noted. Shows flow texture. Moderately altered to clays.	Trachyte	Clays, Quartz Epidote Actinolite
1438-1448	Fine-grained chilled lava. It is relatively fresh with quartz phenocrysts embedded in the groundmass. Slightly altered to fine-grained brown clays.	Rhyolitic intrusion	Clays
1448-1552	Light grey medium-grained highly porphyritic lava. It has phenocrysts of mafic minerals and sanidine. Highly oxidized and altered to brown fine-grained clays.	Trachyte	Clays, Quartz Epidote Prehnite Actinolite
1522-1572	White fine-grained rhyolitic lava. The grains are chilled and show moderate alteration to brown clays.	Rhyolite	Clays, Epidote Actinolite

Depth	Rock description	Rock type	Secondary minerals
1572-1606	White to brown fine- to medium-grained lava. Has mafic minerals forming phenocrysts together with quartz. Moderate to high alteration to fine-grained brown clays. Veins noted filled with epidote and clays.	Rhyolite	Clays, Epidote Wollastonite Actinolite
1606-1732	Fine to medium grey light grey highly porphyritic lava. Phenocrysts of sanidine and plagioclase noted. Veins filled with clays.	Trachyte	Clays, Quartz Epidote Actinolite
1732-1740	Fine- to medium-grained mixture of lava. Rhyolite grains dominate. Trachyte grains are highly porphyritic; tuff grains are lithic in nature. Show moderate alteration.	rhyolite	Clays Epidote Actinolite
1740-1754	Fine- to medium-grained grey brown lava. I t is a mixture of trachytic and rhyolitic grains. Trachytic grains in abundance revealing flow texture. Moderately altered to brown fine-grained clays.	Trachyte	Clays, Quartz Epidote Actinolite
1754-1766	White fine- to medium-grained lava. Phenocrysts of quartz and feldspar in the ground mass. Veins and vesicles noted and filled with quartz, wollastonite and actinolite.	Rhyolite	Clays, Quartz Epidote Actinolite
1766-1774	Light grey medium-grained trachytic lava. It has phenocrysts of feldspars and pyroxenes.	Trachyte	Clays, Quartz Epidote Actinolite
1774-1784	Loss of cuttings	-	-
1784-1886	Light grey medium-grained trachytic lava. It has phenocrysts of feldspars and pyroxenes. Abundant epidote and actinolite.	Trachyte	Clays, Quartz Epidote Actinolite
1888-1892	Greenish to whitish grey fine-grained lava with chilled mineral grains. It has veins filling into which clays have precipitated. It is relatively fresh.	Rhyolitic intrusion	Clays Actinolite
1894-1970	Medium-grained grey to brown lava. Shows high oxidation at 1894-1900. Veins filled with actinolite. It is highly altered to brown fine-grained clays. The lava has a mix of tuff and rhyolite in it. Phenocrysts of feldspars and mafic minerals are abundant revealing flow texture.		Clays, Quartz Epidote Actinolite
1970-1988	Green to dark grey medium-grained lava. Highly porphyritic with abundant mafic phenocrysts. Sphene observed disseminated in the matrix.	Basalt	Clays, Quartz Epidote Prehnite Actinolite
1988-2018	Fined to medium-grained grey lava. It is highly porphyritic with feldspar and quartz phenocrysts. Moderately altered to brown clays. Has veins filled with mafic minerals	Trachyte	Clays, Quartz Epidote Actinolite
1218-2028	Fine-grained whitish grey lava. Characterised by bomb-like mineral fragments and it's highly oxidized and show alteration to brown clays. Quartz phenocrysts noted in the groundmass. The crystals are chilled. It is relatively fresh.	Rhyolitic intrusion	Clays
2028-2208	Light grey medium-grained highly porphyritic lava. It has phenocrysts of mafic minerals and feldspars. It shows moderate alteration to brown clays.	Trachyte	Clays, Quartz Epidote Actinolite
2208-2216	Fine-grained white lava with chilled crystals. It is relatively fresh with veins being filled with green clays.	Rhyolitic intrusion	Clays
2216-2258	Fine- to medium-grained grey highly porphyritic lava. It has feldspar and mafic mineral phenocrysts. It is rich in feldspars. Moderately altered to brown clays.	Trachyte	Clays, Quartz Epidote Actinolite Prehnite
2258-2274	Dark grey to green medium-grained lava. Calcite present in abundance. It has abundant mafic phenocrysts.	Basalt	Clays, Calcite Quartz Epidote Actinolite

Depth	Rock description	Rock type	Secondary minerals
2276-2280	Light grey fine- to medium-grained lava. It has abundant feldspar phenocrysts showing flow texture. Mafic phenocrysts appear in minute quantities. It is slightly altered to brown clays.	Trachyte	Clays, Quartz Epidote Actinolite
2280-2286	Loss of cuttings	-	-
2286-2290	Light grey fine- to medium-grained lava. It has abundant feldspar phenocrysts showing flow texture. Mafic phenocrysts appear in minute quantities. It is slightly altered to brown clays.	Trachyte	Clays, Quartz Epidote Actinolite
2290-2456	Loss of cuttings	-	-
2456-2466	Light to dark grey fine- to medium-grained lava. It has abundant feldspar phenocrysts showing flow texture. Mafic phenocrysts appear in minute quantities. It is highly altered to brown clays. Abundant epidote, wollastonite and actinolite noted.	Trachyte	Clays, Quartz Epidote Actinolite Wollastonite
2466-2470	Loss of cuttings	-	-
2470-2496	Medium-grained whitish grey lava. It is highly porphyritic with feldspars and mafic minerals forming the phenocrysts. Shows slight intensity of alteration to brown clays. Trachytic texture revealed.	Trachyte	Clays, Quartz Epidote Prehnite Actinolite
2496-2516	Fine-grained brown tuffaceous lava. It has rhyolite mineral grains mixed in the sample. Shows high intensity of alteration to brown fine-grained clays.	Tuff	Clays, Quartz Epidote Prehnite Actinolite
2516-2524	Light- to medium-grained light grey lava. It shows slight intensity of alteration. It has quartz phenocrysts in the groundmass.	Rhyolite	Clays, Quartz Epidote Actinolite
2524-2530	Loss of cuttings	-	-
2530-2544	Fine-grained chilled lava. It's relatively fresh with quartz phenocrysts embedded in the groundmass. Slightly altered to fine-grained brown clays.	Rhyolitic intrusion	Clays
2544-2580	Medium-grained whitish grey lava. It is highly porphyritic with feldspars and mafic minerals forming the phenocrysts. Shows slight intensity of alteration to brown clays. Trachytic texture revealed.	Trachyte	Clays, Quartz Epidote Actinolite
2584-2624	Light- to medium-grained light grey lava. It shows slight intensity of alteration. It has quartz phenocrysts in the groundmass.	Rhyolite	Clays, Quartz Epidote Actinolite
2624-2698	Medium-grained whitish grey lava. It is highly porphyritic with feldspars and mafic minerals forming the phenocrysts. Shows moderate intensity of alteration to brown clays. Trachytic texture revealed. Veins are filled with epidote.	Trachyte	Clays, Quartz Epidote Actinolite
2698-2734	Loss of cuttings	-	-
2734-2788	Light grey fine- to medium-grained highly porphyritic lava. It has abundant sanidine phenocrysts and it is highly altered to brown clays.	Trachyte	Clays, Quartz Epidote Actinolite
2788-2794	Loss of cuttings	-	-
2794-2936	Light grey medium-grained moderately porphyritic lava. It is moderately altered to brown clays with sanidine phenocrysts in abundance.	Trachyte	Clays, Quartz Epidote Actinolite
2936-2966	Whitish to greenish fine-grained lava with quartz crystal forming the phenocrysts. It is oxidized to white colour. The crystals are chilled and relatively fresh.	Rhyolitic intrusion	Clays
2966-2996	Medium-grained light grey highly porphyritic lava. It has abundant sanidine phenocrysts and epidote is noted in abundance at 2966. It is highly altered to brown and green fine-grained clays.	Trachyte	Clays, Quartz Epidote Actinolite Prehnite

APPENDIX II: Results of the XRD clay analysis

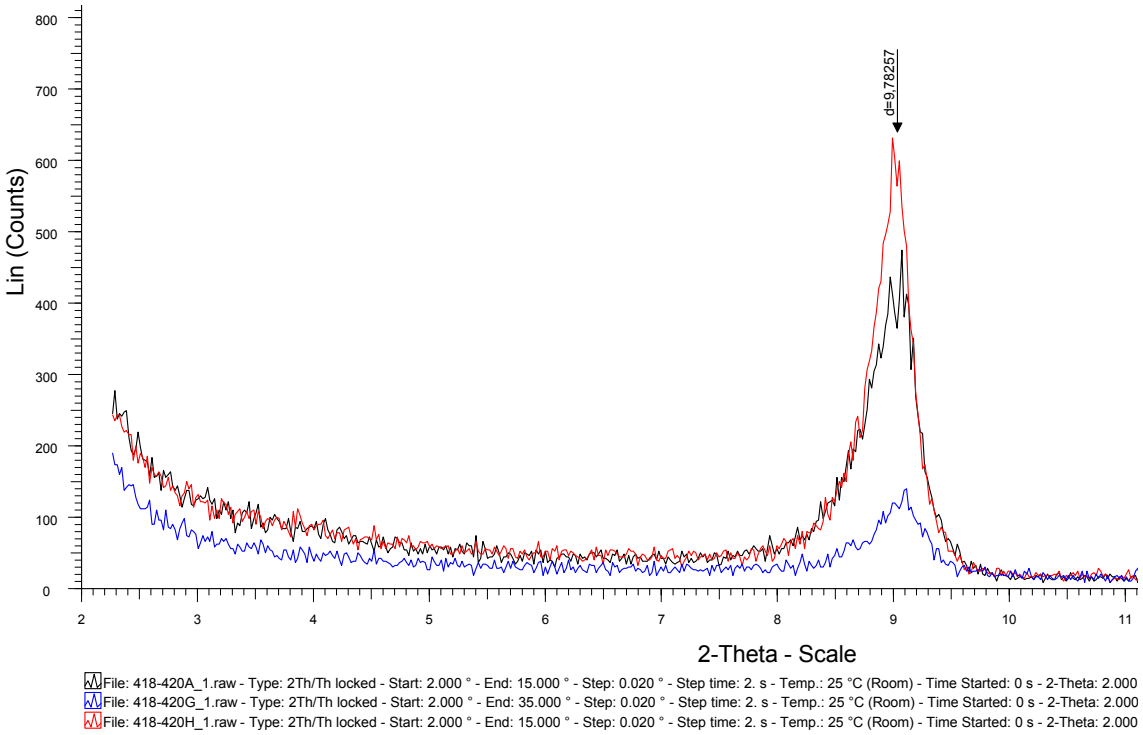

FIGURE 1: Diffractograms of illite clays at 418 m in well OW-914A; peaks at 9.78257Å in untreated (black curve), glycolated (blue curve) and heated (red curve) sample

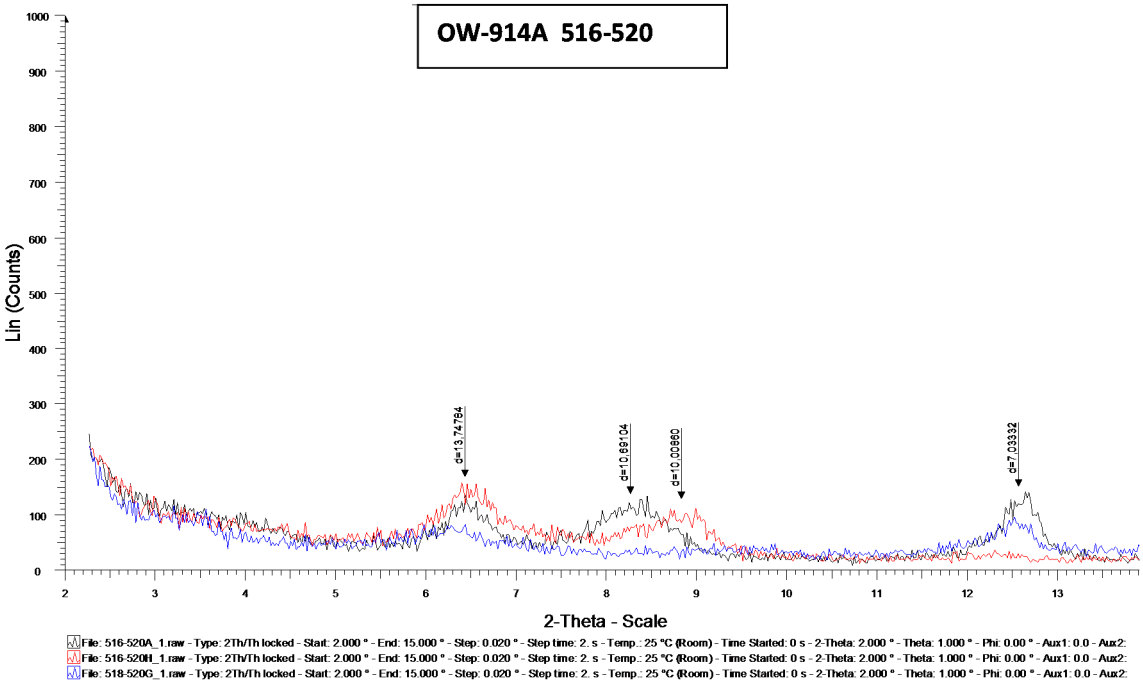

FIGURE 2: Diffractograms of chlorite (unstable) at 516 m in OW-914A; peaks at 13.74784 for chlorite when the sample is untreated, glycolated and heated and the other 7.03332 when the sample is untreated and glycolated but disappears completely when heated

TABLE 1: XRD results

Depth (m)	Results	Depth (m)	Results
18-20	No clay	1198-1200	Illite
78-80	No clay	1238-1240	Illite
178-180	No clay	1258-1260	Illite
238-240	No clay	1398-1400	No clay
278-280	Illite	1438-1440	Illite
398-400	Illite	1478-1480	Illite, feldspar
418-420	Illite	1518-1520	No clay
458-460	Illite	1578-1580	Illite
478-480	Illite	1758-1760	Illite
516-520	Illite	1898-1900	No clay
618-620	Chlorite	1998-2000	Illite
798-800	Chlorite	2058-2060	Illite
1018-1020	Illite	2098-2100	Amphibole
1038-1040	Illite, amphibole	2178-2180	Illite
1058-1060	Illite	2358-2360	Illite
1098-1100	Illite	2398-2400	No clay
1158-1160	No clay		